Inorg. Chem. **2006**, *45*, 1517–1534

Syntheses and X-ray Crystal Structures of α- and β-$[XeO_2F][SbF_6]$, $[XeO_2F][AsF_6]$, $[FO_2XeFXeO_2F][AsF_6]$, and $[XeF_5][SbF_6]\cdot XeOF_4$ and Computational Studies of the XeO_2F^+ and $FO_2XeFXeO_2F^+$ Cations and Related Species

Bernard E. Pointner,[†] Reijo J. Suontamo,[‡] and Gary J. Schrobilgen*[,†]

Department of Chemistry, McMaster University, Hamilton, Ontario L8S 4M1, Canada, and Department of Chemistry, University of Jyväskylä, P.O. Box 35, Jyväskylä FIN-40014, Finland

Received June 22, 2005

Reactions of XeO_2F_2 with the strong fluoride ion acceptors, AsF_5 and SbF_5, in anhydrous HF solvent give rise to α- and β-$[XeO_2F][SbF_6]$, $[XeO_2F][AsF_6]$, and $[FO_2XeFXeO_2F][AsF_6]$. The crystal structures of α-$[XeO_2F][SbF_6]$ and $[XeO_2F][AsF_6]$ consist of trigonal-pyramidal XeO_2F^+ cations, which are consistent with an AXY_2E VSEPR arrangement, and distorted octahedral MF_6^- (M = As, Sb) anions. The β-phase of $[XeO_2F][SbF_6]$ is a tetramer in which the xenon atoms of four XeO_2F^+ cations and the antimony atoms of four SbF_6^- anions are positioned at alternate corners of a cube. The $FO_2XeFXeO_2F^+$ cations of $[FO_2XeFXeO_2F][AsF_6]$ are comprised of two XeO_2F units that are bridged by a fluorine atom, providing a bent Xe- - -F- - -Xe arrangement. The angle subtended by the bridging fluorine atom, a xenon atom, and the terminal fluorine atom of the XeO_2F group is bent toward the valence electron lone-pair domain on xenon, so that each F- - -XeO_2F moiety resembles the AX_2Y_2E arrangement and geometry of the parent XeO_2F_2 molecule. Reaction of XeF_6 with $[H_3O][SbF_6]$ in a 1:2 molar ratio in anhydrous HF predominantly yielded $[XeF_5][SbF_6]\cdot XeOF_4$ as well as $[XeO_2F][Sb_2F_{11}]$. The crystal structure of the former salt was also determined. The energy-minimized, gas-phase MP2 geometries for the XeO_2F^+ and $FO_2XeFXeO_2F^+$ cations are compared with the experimental and calculated geometries of the related species IO_2F, TeO_2F^-, $XeO_2(OTeF_5)^+$, XeO_2F_2, and $XeO_2(OTeF_5)_2$. The bonding in these species has been described by natural bond orbital and electron localization function analyses. The standard enthalpies and Gibbs free energies for reactions leading to XeO_2F^+ and $FO_2XeFXeO_2F^+$ salts from MF_5 (M = As, Sb) and XeO_2F_2 were obtained from Born–Haber cycles and are mildly exothermic and positive, respectively. When the reactions are carried out in anhydrous HF at low temperatures, the salts are readily formed and crystallized from the reaction medium. With the exception of $[XeO_2F][AsF_6]$, the XeO_2F^+ and $FO_2XeFXeO_2F^+$ salts are kinetically stable toward dissociation to XeO_2F_2 and MF_5 at room temperature. The salt, $[XeO_2F][AsF_6]$, readily dissociates to $[FO_2XeFXeO_2F][AsF_6]$ and AsF_5 under dynamic vacuum at 0 °C. The decompositions of XeO_2F^+ salts to the corresponding XeF^+ salts and O_2 are exothermic and spontaneous but slow at room temperature.

Introduction

The xenon(VI) oxide fluorides $XeOF_4$ and XeO_2F_2 form complexes with the strong Lewis acid, fluoride ion acceptors AsF_5 and SbF_5 and are the only high-valent xenon oxide fluoride complexes that have been characterized. Xenon oxide tetrafluoride forms room-temperature-stable 1:2 and 1:1 complexes with SbF_5, which are formulated as $XeOF_4\cdot 2SbF_5$[1–4] and $XeOF_4\cdot SbF_5$.[3,4] Solid-state Raman spectroscopic studies support the ionic formulations $[XeOF_3][SbF_6]$[3,4] and $[XeOF_3][Sb_2F_{11}]$,[2–4] and the ^{19}F[2,5] and ^{129}Xe[6]

* To whom correspondence should be addressed. E-mail: schrobil@mcmaster.ca.
[†] McMaster University.
[‡] University of Jyväskylä.

(1) Selig, H. *Inorg. Chem.* **1966**, *5*, 183.
(2) Gillespie, R. J.; Landa, B.; Schrobilgen, G. J. *J. Chem. Soc., Chem. Commun.* **1972**, 607.
(3) McKee, D. E.; Adams, C. J.; Bartlett, N. *Inorg. Chem.* **1973**, *12*, 1722.
(4) Gillespie, R. J.; Landa, B.; Schrobilgen, G. J. *Inorg. Chem.* **1976**, *15*, 1256.
(5) Gillespie, R. J.; Schrobilgen, G. J. *Inorg. Chem.* **1974**, *13*, 2370.

10.1021/ic0510260 CCC: $33.50
Published on Web 01/27/2006

NMR spectra of $XeOF_4 \cdot 2SbF_5$ in a SbF_5 solvent established the existence of the $XeOF_3^+$ cation in solution. A subsequent ^{17}O and ^{129}Xe NMR study established the existence of the $XeOF_3^+$ cation in the mixed-solvent medium, HF/SbF_5.[7] Although the spectroscopic studies were consistent with a trigonal-bipyramidal $XeOF_3^+$ cation having an AX_3YE VSEPR[8] arrangement in which the electron lone pair of xenon and a fluorine ligand occupy equatorial positions, it was not possible to unambiguously establish whether the oxygen or a second fluorine occupied the third equatorial position and, correspondingly, two fluorine ligands or a fluorine and oxygen ligand occupied the axial positions. A subsequent X-ray crystal structure determination of $[XeOF_3][SbF_6]$ verified the disphenoidal geometry for the $XeOF_3^+$ cation (C_s symmetry), in which the oxygen atom occupies the equatorial position,[7] and represented, until the present study, the only oxide fluoride cation of xenon for which a crystal structure had been determined.

Xenon dioxide difluoride has been shown to form the SbF_5 adduct $XeO_2F_2 \cdot 2SbF_5$, which has been characterized in the solid state by Raman spectroscopy and formulated as $[XeO_2F][Sb_2F_{11}]$.[2,4] The salt is thermodynamically unstable, decomposing to $[XeF][Sb_2F_{11}]$ and O_2 over a period of several months.[4] Dissolution of $[XeO_2F][Sb_2F_{11}]$ in SbF_5 resulted in decomposition to XeF^+ and O_2, which was sufficiently slow to allow the ^{19}F[2,5] and ^{129}Xe[6] NMR spectra of the XeO_2F^+ cation to be obtained. The Raman and NMR spectroscopic findings were consistent with a trigonal-pyramidal XeO_2F^+ cation (C_s point symmetry) corresponding to an AXY_2E VSEPR arrangement.

A more recent synthetic and vibrational study of the fluoride ion donor properties of XeO_2F_2 led to the synthesis of $XeO_2F_2 \cdot AsF_5$ by the reaction of XeO_2F_2 with excess AsF_5 in anhydrous HF at -78 °C.[9] The $2XeO_2F_2 \cdot AsF_5$ complex was similarly prepared[9] by combining stoichiometric amounts of XeO_2F_2 and AsF_5 in anhydrous HF solvent and isolated upon removal of HF or by dynamic pumping on $XeO_2F_2 \cdot AsF_5$ at 0 °C. The results of the Raman spectroscopic characterization of $XeO_2F_2 \cdot AsF_5$ were consistent with the ionic formulation $[XeO_2F][AsF_6]$, in which the XeO_2F^+ cation has a trigonal-pyramidal geometry, in agreement with earlier Raman[2,4] and NMR[2,5,6] spectroscopic studies. The $2XeO_2F_2 \cdot AsF_5$ complex was formulated as $[FO_2XeFXeO_2F][AsF_6]$ based on its Raman spectrum, which was consistent with a Xe- - -F- - -Xe-bridged $FO_2XeFXeO_2F^+$ cation and was assigned under C_{2v} symmetry.[9]

The present paper reports the syntheses of dimorphic $[XeO_2F][SbF_6]$ and the structural characterization of these and previously reported AsF_6^- salts of the XeO_2F^+ and $FO_2XeFXeO_2F^+$ cations and $[XeF_5][SbF_6] \cdot XeOF_4$ by single-crystal X-ray diffraction. Electronic structure calculations have been used to arrive at the energy-minimized gas-phase geometries to assess the nature of the bonding in XeO_2F^+, $FO_2XeFXeO_2F^+$, and closely related species and to account for the thermodynamic stabilities of XeO_2F^+ and $FO_2XeFXeO_2F^+$ salts.

Results and Discussion

Syntheses of α- and *β*-$[XeO_2F][SbF_6]$, $[XeO_2F][AsF_6]$, $[FO_2XeFXeO_2F][AsF_6]$, and $[XeF_5][SbF_6] \cdot XeOF_4$. The salts α-$[XeO_2F][SbF_6]$ and $[XeO_2F][AsF_6]$ were prepared in anhydrous HF solvent by the reaction of stoichiometric amounts of XeO_2F_2 and MF_5 (M = As and Sb) and were obtained as very pale-yellow to white solids upon removal of the HF solvent (eq 1). The solids were shown by Raman

$$XeO_2F_2 + MF_5 \rightarrow [XeO_2F][MF_6] \quad (1)$$

spectroscopy to be $[XeO_2F][MF_6]$ by comparison of their Raman spectra with those of $[XeO_2F][AsF_6]$[9] and $[XeO_2F][Sb_2F_{11}]$.[2,4]

Although the previous and present works have shown that $[XeO_2F][Sb_2F_{11}]$ can be prepared by the reaction of stoichiometric amounts of XeO_2F_2 and SbF_5 in HF followed by removal of the solvent under vacuum at low temperature (eq 2), it was not possible to crystallize $[XeO_2F][Sb_2F_{11}]$ from HF at low temperatures. When XeO_2F_2 and SbF_5 were

$$XeO_2F_2 + 2SbF_5 \rightarrow [XeO_2F][Sb_2F_{11}] \quad (2)$$

allowed to react in 1:2, 1:3, and 1:4 molar ratios in anhydrous HF at room temperature, the compound that consistently crystallized from HF solution between -45 and -78 °C was the tetrameric *β*-$[XeO_2F][SbF_6]$ phase (see the X-ray Crystal Structures section).

A further attempt was made to prepare and crystallize an $Sb_2F_{11}^-$ salt of the XeO_2F^+ cation by the reaction of $[H_3O][SbF_6]$ with XeF_6 at 0 °C in HF solvent according to eq 3.

$$XeF_6 + 2[H_3O][SbF_6] \rightarrow [XeO_2F][Sb_2F_{11}] + 6HF \quad (3)$$

$$2XeF_6 + [H_3O][SbF_6] \rightarrow [XeF_5][SbF_6] \cdot XeOF_4 + 3HF \quad (4)$$

The Raman spectrum of the isolated solid showed $[XeF_5][SbF_6] \cdot XeOF_4$[10] as the major product (eq 4), $[XeO_2F][SbF_6]$[2,4] (ca. 20% of the xenon-containing product), and unreacted $[H_3O][SbF_6]$. An earlier study[10] had shown that the reaction between liquid $XeOF_4$ and $[KrF][SbF_6]$ yielded a mixture of $[O_2][SbF_6]$ and $[XeF_5][SbF_6] \cdot XeOF_4$ and resulted in the characterization of $[XeF_5][SbF_6] \cdot XeOF_4$ by Raman spectroscopy in the solid state and by ^{19}F NMR spectroscopy in HF solvent.

The previous preparation of $[FO_2XeFXeO_2F][AsF_6]$ entailed the reaction of stoichiometric amounts of XeO_2F_2 and AsF_5 in HF solvent. In the prior[9] and present studies, the $[FO_2XeFXeO_2F][AsF_6]$ salt was also prepared by dynamic pumping on solid $[XeO_2F][AsF_6]$ at 0 °C. The high-dissociation vapor pressure of $[XeO_2F][AsF_6]$ (ca. 7 Torr at 23 °C)[9] resulted in rapid AsF_5 loss under dynamic vacuum (eq 5). The resulting pale-yellow solid was identified as $[FO_2$-

$$2[XeO_2F][AsF_6] \rightarrow [FO_2XeFXeO_2F][AsF_6] + AsF_5 \quad (5)$$

(6) Schrobilgen, G. J.; Holloway, J. H.; Granger, P.; Brevard, C. *Inorg. Chem.* **1978**, *17*, 980.
(7) Mercier, H. P. A.; Sanders, J. C. P.; Schrobilgen, G. J.; Tsai, S. S. *Inorg. Chem.* **1993**, *32*, 386.
(8) Gillespie, R. J.; Hargittai, I. In *The VSEPR Model of Molecular Geometry*; Allyn and Bacon: Boston, MA, 1991.
(9) Christe, K. O.; Wilson, W. W. *Inorg. Chem.* **1988**, *27*, 2714.

Table 1. Summary of Crystal Data and Refinement Results for α- and β-$[XeO_2F][SbF_6]$, $[XeO_2F][AsF_6]$, $[FO_2XeFXeO_2F][AsF_6]$, and $[XeF_5][SbF_6]\cdot XeOF_4$

	α-$[XeO_2F][SbF_6]$	β-$[XeO_2F][SbF_6]$	$[XeO_2F][AsF_6]$	$[FO_2XeFXeO_2F][AsF_6]$	$[XeF_5][SbF_6]\cdot XeOF_4$
space group	$P2_1/c$ (No. 14)	$R3$ (No. 146)	$P2_12_12_1$ (No. 19)	$P2_1/c$ (No. 14)	$P2_1/m$ (No. 11)
a (Å)	10.190(4)	12.9188(9)	8.658(6)	10.488(4)	5.6586(2)
b (Å)	5.719(2)	12.9188(9)	8.699(6)	5.340(2)	8.6566(4)
c (Å)	12.082(4)	14.661(2)	8.916(6)	18.346(6)	12.4042(2)
α (deg)	90	90	90	90	90
β (deg)	92.456(4)	90	90	101.168(5)	102.718(2)
γ (deg)	90	120	90	90	90
V (Å^3)	703.5(4)	2119.1(3)	671.5(8)	1008.1(6)	592.70(4)
Z (molecules/unit cell)	4	3	4	4	2
mol wt (g mol^{-1})	418.05	1672.20	371.22	572.52	685.35
ρ_{calcd} (g cm^{-3})	3.947	3.931	3.672	3.772	3.840
T (°C)	−115	−127	−173	−113	−122
μ (mm^{-1})	8.748	8.713	10.118	10.116	8.134
λ (Å)	0.710 73	0.710 73	0.710 73	0.710 73	0.710 73
R_1[a]	0.0203	0.0445	0.0572	0.0329	0.0160
wR_2[b]	0.0535	0.0700	0.1140	0.0760	0.0416

[a] $R_1 = \sum||F_o| - |F_c|/\sum|F_o|$. [b] $wR_2 = \sum|(|F_o| - |F_c|)w^{1/2}|/\sum(|F_o|w)$.

$XeFXeO_2F][AsF_6]$ by Raman spectroscopy[9] and was further characterized in the present study by an X-ray crystal structure determination.

X-ray Crystal Structures. Details of the data collection parameters and other crystallographic information for α-$[XeO_2F][SbF_6]$, β-$[XeO_2F][SbF_6]$, $[XeO_2F][AsF_6]$, $[FO_2XeFXeO_2F][AsF_6]$, and $[XeF_5][SbF_6]\cdot XeOF_4$ are provided in Table 1, and important bond lengths, bond angles, and significant contacts are listed in Table 2. The bond valencies[11−13] for the primary and secondary contacts of all structures have been calculated and are also listed in Table 2. The xenon atoms of XeO_2F^+, $FO_2XeFXeO_2F^+$, and XeF_5^+ exhibit bond valencies that are significantly less than 6 when only primary bonding interactions are taken into account. When the bond valence contributions from both primary and secondary contacts are included, the total bond valencies are close to 6, as expected for xenon(VI). In the case of α-$[XeO_2F][SbF_6]$, the total bond valence of xenon (5.72) is less than those in $FO_2XeFXeO_2F^+$ (5.95 and 6.01), indicating that xenon in XeO_2F^+ is somewhat undercoordinated relative to xenon in $FO_2XeFXeO_2F^+$.

(a) α-$[XeO_2F][SbF_6]$. The crystal structure of α-$[XeO_2F][SbF_6]$ consists of discreet XeO_2F^+ cations and SbF_6^- anions that interact by means of secondary fluorine bridge contacts (Figure 1a). The primary coordination of the XeO_2F^+ cation is a trigonal-pyramidal arrangement of the oxygen atoms and a fluorine atom. The cation geometry is consistent with an AXY_2E VSEPR arrangement of a single-bond domain (X), two double-bond domains (Y), and a lone-pair domain (E).

The Xe−F bond of XeO_2F^+ is shorter, within $\pm 3\sigma$, than that in $XeOF_4$ [1.900(5) Å;[14] 1.901(3)−1.9040(0) Å;[15] 1.895(2) and 1.890(2) Å[16]] and XeO_2F_2 [1.899(3) Å;[17] 1.892(13) and 1.925(13) Å[18]] and intermediate with respect to Xe−F_{ax} [1.879(12) Å] and Xe−F_{eq} [1.821(12) Å] in $XeOF_3^+$.[7] The net positive charge of the XeO_2F^+ cation leads to a shorter and less polar Xe−F bond. The Xe−O bond lengths in the XeO_2F^+ cation are similar to those observed for other xenon(VI) oxide fluorides [$XeOF_4$, 1.703(15),[14] 1.7053(9)−1.711(11),[15] and 1.713(3) Å;[16] $XeOF_3^+$, 1.692(13) Å;[7] XeO_2F_2, 1.714(4)[17] and 1.731(9) Å;[18] XeO_3, 1.76(2) Å[19]]. Although it is not possible to differentiate between the Xe−O bond lengths obtained for XeO_2F_2 and the XeO_2F^+ cation by diffraction methods, the higher symmetric and antisymmetric XeO_2 stretching frequencies suggest that if they are essentially pure vibrational modes, the Xe−O bonds of XeO_2F^+ (867 and 923 cm^{-1};[4] 873 and 931 cm^{-1} [8]) are shorter and less polar than those of XeO_2F_2 (845−850 and 882−905 cm^{-1}).[20] The O(1)−Xe(1)−O(2), O(1)−Xe(1)−F(7), and O(2)−Xe(1)−F(7) bond angles of the XeO_2F^+ cation are considerably less than the ideal tetrahedral angle as a result of increased repulsion from the lone pair on xenon. A comparison of the O−Xe−O angle of XeO_2F^+ with the corresponding angles in isoelectronic IO_2F[21] and TeO_2F^- [22] (Table S1) shows that the O−E−O (E = Xe, I, Te) bond angles decrease over the series $XeO_2F^+ > IO_2F > TeO_2F^-$. Although IO_2F and TeO_2F^- are oxygen-bridged and XeO_2F^+ is fluorine-bridged in the solid state (Table S1), they form longer and more polar bonds with increasing negative charge. As expected, the volume of the valence electron lone pair on E also increases (see the Natural Bond Orbital and Electron Localization Function Analyses section). This leads to decreased bond pair−bond pair and increased lone pair−bond pair repulsions and contraction of the O−E−O angles along the series.

(10) Holloway, J. H.; Schrobilgen, G. J. *J. Chem. Soc., Chem. Commun.* **1975**, 623.
(11) Brown, I. D. *J. Solid State Chem.* **1974**, *11*, 214.
(12) Brown, I. D. In *Structure and Bonding in Crystals*; O'Keefe, M., Navrotsky, A., Eds.; Academic Press: London, 1981; Vol. 2, p 1.
(13) Brown, I. D.; Altermatt, D. *Acta Crystallogr.* **1985**, *B41*, 244.
(14) Martins, J. F.; Wilson, E. B., Jr. *J. Mol. Spectrosc.* **1968**, *26*, 410.
(15) Jacob, E. J.; Thompson, H. B.; Bartell, L. S. *J. Mol. Struct.* **1971**, *8*, 383.
(16) This work.
(17) Peterson, S. W.; Willett, R. D.; Huston, J. L. *J. Chem. Phys.* **1973**, *59*, 453.
(18) LeBlond, N.; Dixon, D. A.; Schrobilgen, G. J. *Inorg. Chem.* **2000**, *39*, 2473.
(19) Templeton, D. H.; Zalkin, A.; Forrester, J. D.; Williamson, S. M. *J. Am. Chem. Soc.* **1963**, *85*, 817.
(20) Claassen, H. H.; Gasner, E. L.; Kim, H.; Huston, J. L. *J. Chem. Phys.* **1968**, *49*, 253.
(21) Minkwitz, R.; Berkei, M.; Ludwig, R. *Inorg. Chem.* **2001**, *40*, 6493.
(22) Kessler, U.; Jansen, M. *Eur. J. Inorg. Chem.* **2000**, 1767.

Table 2. Bond Lengths (Å), Bond Angles (deg), Contacts (Å), and Bond Valencies in α- and *β*-$[XeO_2F][SbF_6]$, $[XeO_2F][AsF_6]$, $[FO_2XeFXeO_2F][AsF_6]$, and $[XeF_5][SbF_6]\cdot XeOF_4$

α-$[XeO_2F][SbF_6]$

Bond Lengths (Å), Contacts (Å), and Bond Valencies (vu)[a]

Xe(1)−O(1)	1.740(3) [2.019]	Xe(1)−O(2)	1.726(3) [2.091]	Xe(1)−F(7)	1.849(2) [1.117]
Xe(1)···F(6C)	2.590(2) [0.151]	Xe(1)···F(5)	2.614(2) [0.141]	Xe(1)···F(1B)	2.671(2) [0.121]
Xe(1)···F(3A)	2.969(3) [0.054]	Xe(1)···F(4D)	3.276(3) [0.024]		
total bond valence: 5.718					
Sb(1)−F(1)	1.891(2)	Sb(1)−F(2)	1.863(2)	Sb(1)−F(3)	1.865(2)
Sb(1)−F(4)	1.863(2)	Sb(1)−F(5)	1.896(2)	Sb(1)−F(6)	1.906(2)

Bond Angles and Contact Bond Angles (deg)

O(1)−Xe(1)−O(2)	105.0(2)	O(1)−Xe(1)−F(7)	95.7(1)	O(2)−Xe(1)−F(7)	98.2(1)
O(1)−Xe(1)···F(6C)	80.4(1)	O(1)−Xe(1)···F(5)	84.5(1)	O(1)−Xe(1)···F(1B)	156.9(1)
O(2)−Xe(1)···F(6C)	85.2(1)	O(2)−Xe(1)···F(5)	169.4(1)	O(2)−Xe(1)···F(1B)	95.8(1)
F(7)−Xe(1)···F(6C)	175.4(1)	F(7)−Xe(1)···F(5)	76.1(1)	F(7)−Xe(1)···F(1B)	71.11(9)
F(6C)···Xe(1)···F(5)	101.06(8)	F(6C)···Xe(1)···F(1B)	111.7(7)	F(5)···Xe(1)···F(1B)	74.02(7)
F(1)−Sb(1)−F(2)	89.3(1)	F(1)−Sb(1)−F(3)	88.1(1)	F(1)−Sb(1)−F(4)	178.4(1)
F(1)−Sb(1)−F(5)	88.8(1)	F(1)−Sb(1)−F(6)	89.1(1)	F(2)−Sb(1)−F(3)	177.4(1)
F(2)−Sb(1)−F(4)	92.2(1)	F(2)−Sb(1)−F(5)	88.9(1)	F(2)−Sb(1)−F(6)	89.0(1)
F(3)−Sb(1)−F(4)	90.3(1)	F(3)−Sb(1)−F(5)	90.8(1)	F(3)−Sb(1)−F(6)	91.3(1)
F(4)−Sb(1)−F(5)	91.3(1)	F(4)−Sb(1)−F(6)	90.8(1)	F(5)−Sb(1)−F(6)	177.0(1)

$[XeO_2F][AsF_6]$

Bond Lengths and Contacts (Å)

Xe(1)−O(1)	1.740(10)	Xe(1)−O/F(2)	1.765(8)	Xe(1)−O/F(3)	1.777(8)
Xe(1)···F(2)	2.602(7)	Xe(1)···F(5A)	2.618(8)	Xe(1)···F(6A)	2.718(8)
Xe(1)···F(1A)	3.028(8)				
As(1)−F(1)	1.709(8)	As(1)−F(2)	1.739(7)	As(1)−F(3)	1.695(9)
As(1)−F(4)	1.701(8)	As(1)−F(6)	1.735(7)	As(1)−F(5)	1.753(8)

Bond Angles and Contact Bond Angles (deg)

O(1)−Xe(1)−O/F(2)	101.9(4)	O(1)−Xe(1)−O/F(3)	101.3(4)	O/F(2)−Xe(1)−O/F(3)	98.9(4)
O(1)−Xe(1)···F(2)	93.6(4)	O(1)−Xe(1)···F(5A)	168.5(4)	O(1)−Xe(1)···F(6A)	100.8(4)
O/F(2)−Xe(1)···F(2)	164.5(3)	O/F(2)−Xe(1)···F(5A)	85.3(3)	O/F(2)−Xe(1)···F(6A)	76.9(4)
O/F(3)−Xe(1)···F(2)	77.8(3)	O/F(3)−Xe(1)···F(5A)	86.3(4)	O/F(3)−Xe(1)···F(6A)	157.9(3)
F(2)···Xe(1)···F(5A)	79.5(2)	F(2)···Xe(1)···F(6A)	100.4(2)	F(5A)···Xe(1)···F(6A)	71.9(2)
F(1)−As(1)−F(2)	90.7(4)	F(1)−As(1)−F(3)	90.8(4)	F(1)−As(1)−F(4)	176.0(4)
F(1)−As(1)−F(5)	87.5(4)	F(1)−As(1)−F(6)	86.9(4)	F(2)−As(1)−F(3)	91.5(4)
F(2)−As(1)−F(4)	91.5(4)	F(2)−As(1)−F(5)	88.0(4)	F(2)−As(1)−F(6)	176.2(4)
F(3)−As(1)−F(4)	92.6(4)	F(3)−As(1)−F(5)	178.2(4)	F(3)−As(1)−F(6)	91.5(4)
F(4)−As(1)−F(5)	89.3(4)	F(4)−As(1)−F(6)	90.7(4)	F(5)−As(1)−F(6)	88.9(4)

***β*-$[XeO_2F][SbF_6]$**

Bond Lengths and Contacts (Å)

Xe(1)−O/F(1)	1.798(12)	Xe(1)−O/F(2)	1.814(17)	Xe(1)−O/F(3)	1.745(12)
Xe(1)···F(9B)	2.533(12)	Xe(1)···F(10)	2.549(12)	Xe(1)···F(11)	2.576(11)
Xe(2)−F/O(4)	1.756(16)	Xe(2)···F(8)	2.571(10)		
Sb(1)−F(5)	1.841(13)	Sb(1)−F(6)	1.819(15)	Sb(1)−F(7)	1.882(12)
Sb(1)−F(8)	1.914(10)	Sb(1)−F(9)	1.919(12)	Sb(1)−F(10)	1.956(12)
Sb(2)−F(11)	1.881(11)	Sb(2)−F(12)	1.869(16)		

Bond Angles and Contact Bond Angles (deg)

O/F(1)−Xe(1)−O/F(2)	100.8(7)	O/F(1)−Xe(1)−O/F(3)	100.0(7)	O/F(1)−Xe(1)−F(9B)	162.1(6)
O/F(1)−Xe(1)···F(10)	86.5(5)	O/F(1)−Xe(1)···F(11)	85.8(5)	O/F(2)−Xe(1)−O/F(3)	103.1(7)
O/F(2)−Xe(1)···F(9B)	92.4(6)	O/F(2)−Xe(1)···F(10)	167.5(6)	O/F(2)−Xe(1)···F(11)	88.4(6)
O/F(3)−Xe(1)···F(9B)	88.6(6)	O/F(3)−Xe(1)···F(10)	85.4(5)	O/F(3)−Xe(1)···F(11)	165.8(5)
F(9B)···Xe(1)···F(10)	78.5(4)	F(9B)···Xe(1)···F(11)	82.5(4)	F(10)···Xe(1)···F(11)	82.0(3)
O/F(4)−Xe(2)−O/F(4A)	102.7(6)	O/F(4)−Xe(2)···F(8)	162.5(6)	O/F(4)−Xe(2)···F(8A)	89.6(5)
O/F(4)−Xe(2)···F(8B)	86.4(5)	F(8)···Xe(2)···F(8A)	78.6(4)		
F(5)−Sb(1)−F(6)	93.9(6)	F(5)−Sb(1)−F(7)	92.2(5)	F(5)−Sb(1)−F(8)	90.6(5)
F(5)−Sb(1)−F(9)	89.7(5)	F(5)−Sb(1)−F(10)	174.9(6)	F(6)−Sb(1)−F(7)	91.7(6)
F(6)−Sb(1)−F(8)	91.1(6)	F(6)−Sb(1)−F(9)	174.8(7)	F(6)−Sb(1)−F(10)	90.2(5)
F(7)−Sb(1)−F(8)	175.9(6)	F(7)−Sb(1)−F(9)	91.9(6)	F(7)−Sb(1)−F(10)	90.6(5)
F(8)−Sb(1)−F(9)	85.1(5)	F(8)−Sb(1)−F(10)	86.5(5)	F(9)−Sb(1)−F(10)	86.0(5)
F(11)−Sb(2)−F(11A)	87.6(5)	F(11)−Sb(2)−F(12)	89.8(5)	F(11)−Sb(2)−F(12A)	91.0(5)
F(11)−Sb(2)−F(12B)	177.1(6)	F(12)−Sb(2)−F(12A)	91.5(6)		
Xe(1)···F(10)−Sb(1)	169.5(6)	Xe(1)···F(11)−Sb(2)	172.8(7)	Xe(2)···F(8)−Sb(1)	169.3(6)

$[FO_2XeFXeO_2F][AsF_6]$

Bond Lengths (Å), Contacts (Å), and Bond Valencies (vu)[a]

Xe(1)−O(1)	1.719(4) [2.137]	Xe(1)−O(2)	1.719(4) [2.137]	Xe(1)−F(7)	1.870(4) [1.053]
Xe(1)···F(8)	2.161(3) [0.481]	Xe(1)···F(3A)	2.768(4) [0.093]	Xe(1)···F(2A)	2.713(4) [0.108]
Xe(2)−O(3)	1.715(4) [2.160]	Xe(2)−O(4)	1.721(4) [2.126]	Xe(2)−F(9)	1.872(3) [1.050]
Xe(2)···F(8)	2.230(3) [0.399]	Xe(2)···F(4A)	2.791(4) [0.088]	Xe(2)···F(5)	2.659(4) [0.125]
total bond valence: 6.009 [Xe(1)] and 5.948 [Xe(2)]					
As(1)−F(1)	1.672(4)	As(1)−F(2)	1.726(4)	As(1)−F(3)	1.731(4)
As(1)−F(4)	1.727(3)	As(1)−F(5)	1.727(4)	As(1)−F(6)	1.699(4)

Table 2. Cont'd.

		$[FO_2XeFXeO_2F][AsF_6]$			
		Bond Angles and Contact Bond Angles (deg)			
O(1)−Xe(1)−O(2)	105.8(2)	O(1)−Xe(1)−F(7)	95.2(2)	O(1)−Xe(1)···F(8)	91.1(2)
O(2)−Xe(1)−F(7)	95.6(2)	O(2)−Xe(1)···F(8)	90.6(2)	F(7)−Xe(1)···F(8)	169.7(2)
O(1)−Xe(1)···F(3A)	167.5(2)	O(1)−Xe(1)···F(2A)	84.0(2)	O(2)−Xe(1)···F(3A)	84.2(2)
O(2)−Xe(1)···F(2A)	168.5(2)	F(7)−Xe(1)···F(3A)	91.3(2)	F(7)−Xe(1)···F(2A)	89.3(2)
F(8)···Xe(1)···F(3A)	81.1(1)	F(8)···Xe(1)···F(2A)	83.2(1)	F(3A)···Xe(1)···F(2A)	85.3(1)
O(3)−Xe(2)−O(4)	105.8(2)	O(3)−Xe(2)···F(8)	89.9(2)	O(3)−Xe(2)−F(9)	96.0(2)
O(4)−Xe(2)···F(8)	89.8(2)	O(4)−Xe(2)−F(9)	95.4(2)	F(9)−Xe(2)···F(8)	170.8(2)
O(3)−Xe(2)···F(4A)	169.2(2)	O(3)−Xe(2)···F(5)	85.2(2)	O(4)−Xe(2)···F(4A)	82.8(2)
O(4)−Xe(2)···F(5)	166.8(2)	F(9)−Xe(2)···F(4A)	76.4(1)	F(9)−Xe(2)···F(5)	75.8(1)
F(8)···Xe(2)···F(4A)	96.8(1)	F(8)···Xe(2)···F(5)	97.8(1)	F(4A)···Xe(2)···F(5)	85.6(1)
Xe(1)−F(8)−Xe(2)	166.4(2)				
F(1)−As(1)−F(2)	90.8(2)	F(1)−As(1)−F(3)	89.6(2)	F(1)−As(1)−F(4)	91.8(2)
F(1)−As(1)−F(5)	89.9(2)	F(1)−As(1)−F(6)	179.6(2)	F(2)−As(1)−F(3)	89.7(2)
F(2)−As(1)−F(4)	90.5(2)	F(2)−As(1)−F(5)	178.8(2)	F(2)−As(1)−F(6)	89.2(2)
F(3)−As(1)−F(4)	178.5(2)	F(3)−As(1)−F(5)	89.4(2)	F(3)−As(1)−F(6)	89.9(2)
F(4)−As(1)−F(5)	90.4(2)	F(4)−As(1)−F(6)	88.6(2)	F(5)−As(1)−F(6)	90.1(2)
		$[XeF_5][SbF_6]\cdot XeOF_4$			
		Bond Lengths (Å), Contacts (Å), and Bond Valencies (vu)[a]			
Xe(1)−O(1)	1.713(3) [2.172]	Xe(1)−F(1)	1.890(2) [1.001]	Xe(1)−F(2)	1.895(2) [0.987]
Xe(1)···F(7)	2.840(2) [0.077]	Xe(2)−F(4)	1.818(2) [1.215]	Xe(2)−F(5)	1.851(2) [1.111]
Xe(2)−F(3)	1.840(2) [1.145]	Xe(2)···F(8)	2.592(2) [0.150]	Xe(2)···F(9A)	2.658(2) [0.125]
Xe(2)···F(6B)	3.070(2) [0.041]	Xe(2)···F(6C)	3.070(2) [0.041]		
total bond valence: 6.225 ($XeOF_4$) and 6.161 (XeF_5^+)					
Sb(1)−F(6)	1.880(2)	Sb(1)−F(7)	1.880(2)	Sb(1)−F(8)	1.906(2)
Sb(1)−F(9)	1.903(2)	Sb(1)−F(10)	1.862(2)		
		Bond Angles (deg)			
O(1)−Xe(1)−F(1)	90.7(1)	O(1)−Xe(1)−F(2)	90. 6(1)	F(1)−Xe(1)−F(2)	89.8(1)
F(1)−Xe(1)−F(2A)	178.74(9)	F(4)−Xe(2)−F(3)	80.29(8)	F(4)−Xe(2)−F(5)	80.13(8)
F(3)−Xe(2)−F(5)	88.98(8)	F(4)−Xe(2)−F(3A)	80.29(8)	F(4)−Xe(2)−F(5A)	80.13(8)
F(3A)−Xe(2)−F(5A)	88.98(8)	F(3A)−Xe(2)−F(5)	160.43(8)	F(3)−Xe(2)−F(5A)	160.43(8)
F(6)−Sb(1)−F(6A)	175.9(1)	F(6)−Sb(1)−F(7)	90.02(5)	F(6)−Sb(1)−F(8)	87.94(5)
F(6)−Sb(1)−F(9)	89.87(5)	F(6)−Sb(1)−F(10)	92.05(5)	F(7)−Sb(1)−F(8)	89.8(1)
F(7)−Sb(1)−F(9)	177.0(1)	F(7)−Sb(1)−F(10)	91.7(1)	F(8)−Sb(1)−F(9)	87.19(9)
F(8)−Sb(1)−F(10)	178.5(1)	F(9)−Sb(1)−F(10)	91.3(1)		

[a] Bond valencies are given in square brackets. Bond valence units (vu) are defined in refs 11−13. The most recent values for xenon(VI) have been used and are personal communications from I. D. Brown, Department of Chemistry, McMaster University. $R_0(Xe^{VI}-O) = 2.00$, $R_0(Xe^{VI}-F) = 1.89$, and $B = 0.37$.

When viewed along the *b*-axis, in the direction of the *a*-axis (Figure 1b), a projection of the packing of α-$[XeO_2F][SbF_6]$ shows a two-dimensional, layered structure in which double layers of XeO_2F^+ cations are sandwiched between double layers of SbF_6^- anions. The xenon atom of each XeO_2F^+ cation has five nonequivalent secondary fluorine bridge contacts to five different SbF_6^- anions. The shortest of the contacts are Xe(1)···F(5), 2.614(2) Å, Xe(1)···F(1B), 2.671(2) Å, and Xe(1)···F(6C), 2.590(2) Å, which are significantly less than the sum of the Xe and F van der Waals radii (3.63 Å),[23] indicating that these secondary contacts have substantial covalent character. The secondary contacts give rise to a distorted monocapped octahedral environment about the xenon atom that is consistent with an AXY_2Z_3E VSEPR arrangement of one primary single-bond domain (X), two primary double-bond-pair domains (Y), three secondary single-bond domains (Z), and one electron lone-pair domain (E). Two significantly longer Xe···F interactions are also observed, Xe(1)···F(3A), 2.969(3) Å, and Xe(1)···F(4D), 3.276(3) Å, bringing the total coordination number of xenon to 9. These contacts enter the coordination sphere of xenon from above the distorted O(1)−O(2)−F(5)−F(1B) plane and imply that the location of the electron lone pair lies in the triangular F(1B)−F(3A)−F(4D) face. The directions of the secondary contacts are similar to those in the structure of IO_2F.[21]

The SbF_6^- anions of α-$[XeO_2F][SbF_6]$ have distorted octahedral geometries with Sb−F bond lengths ranging from 1.863(2) to 1.906(2) Å. The lengthening of some Sb−F bonds is attributed to interactions of the fluorine atoms on antimony with neighboring xenon centers (vide supra). The bridging fluorine atom, F(6), exhibits the shortest of the secondary contacts to xenon [2.590(2) Å] and, as expected, the Sb−F(6) bond [1.906(2) Å] is the longest Sb−F bond. The remaining longer fluorine bridge contacts to xenon and their corresponding Sb−F bond lengths demonstrate that Sb−F bond elongation attenuates with increasing Xe···F distance (Table 2).

(b) $[XeO_2F][AsF_6]$. The crystal structure of $[XeO_2F][AsF_6]$ was determined from a racemic twin crystal that also exhibited cubic twinning, inducing a positional disorder between one oxygen and the fluorine atom of the XeO_2F^+ cation. The disorder did not allow the extraction of discreet Xe−O and Xe−F bond lengths and angles for the oxygen and fluorine atoms that are involved in the disorder but did

(23) Bondi, A. *J. Phys. Chem.* **1964**, *68*, 441.

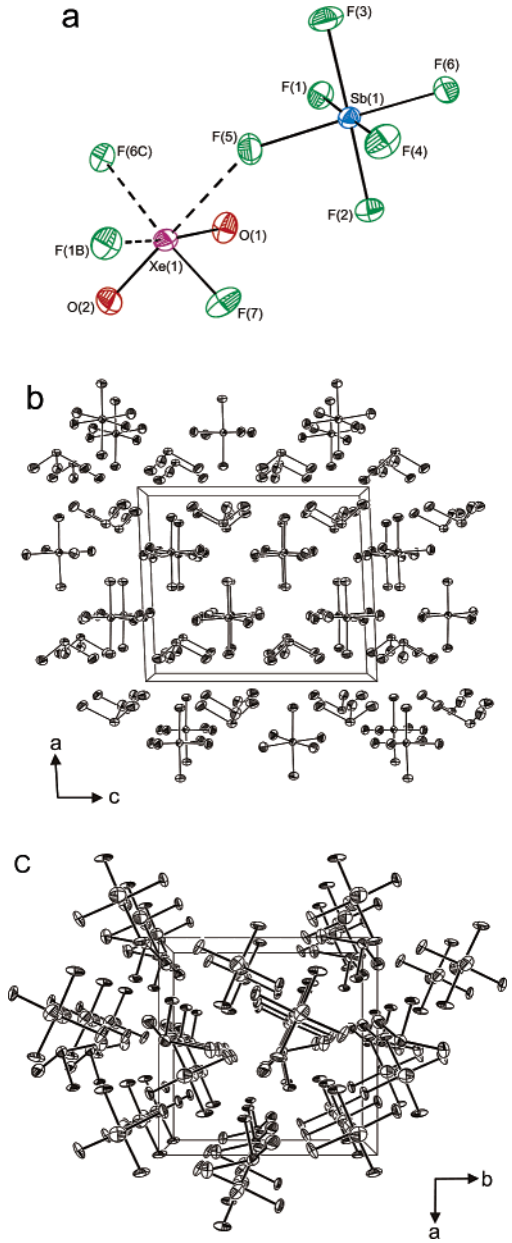

Figure 1. (a) X-ray crystal structure of α-[XeO_2F][SbF_6]. Thermal ellipsoids are shown at the 50% probability level. (b) Packing of α-[XeO_2F]-[SbF_6] along the *b*-axis. (c) Packing of [XeO_2F][AsF_6] along the *c*-axis.

provide a reliable Xe(1)−O(1) bond length. The disordered Xe−O/F bond lengths are in good agreement with the weighted average of the Xe−O and Xe−F bond lengths obtained from the ordered α-[XeO_2F][SbF_6] structure. The structural unit and secondary coordination spheres of xenon in [XeO_2F][AsF_6] are similar to those of α-[XeO_2F][SbF_6] and require no further comment. The AsF_6^- anions have distorted octahedral geometries similar to those of the SbF_6^- anion in α-[XeO_2F][SbF_6] and also require no further comment.

The crystal packing of [XeO_2F][AsF_6] (Figure 1c) differs from that of α-[XeO_2F][SbF_6] (Figure 1b). The XeO_2F^+ cations and AsF_6^- anions form columns of alternating cations and anions when viewed along the *c*-axis, whereas α-[XeO_2F]-[SbF_6] is a layered structure when viewed along any axis.

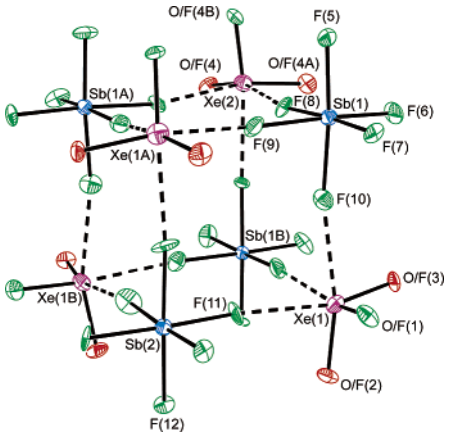

Figure 2. X-ray crystal structure of *β*-[XeO_2F][SbF_6]. Thermal ellipsoids are shown at the 50% probability level. The symmetry-equivalent atoms are not labeled.

(c) *β*-[XeO_2F][SbF_6]. The unit cell of *β*-[XeO_2F][SbF_6] consists of three tetrameric units. The xenon and antimony atoms of each tetrameric unit occupy alternate vertices of a cube (Figure 2). The compound crystallizes in the space group *R*3 with the 3-fold axis of the unit cell passing through Xe(2) and Sb(2) and, as a result, the fluorine and oxygen atoms bonded to xenon are positionally disordered. The average Xe−O/F bond lengths in the tetramer bracket the weighted average of the Xe−O and Xe−F bond lengths obtained for the ordered α-phase (1.772 Å). The Xe(1) atom has three secondary contacts to fluorine atoms of three SbF_6^- anions that are ∼1 Å less than the sum of the xenon and fluorine van der Waals radii (Table 2). The Xe(2) atom also has three similar contacts to fluorine atoms of the SbF_6^- anions that are equivalent by crystal symmetry (Table 2).

Although the exterior O/F−Xe(1)−O/F and O/F−Xe(2)−O/F angles are significantly more open by 17−24° than the interior angles formed by the interior Xe···F contacts, they are sufficiently long to allow accommodation of the xenon valence electron lone pairs between Xe(1)···F(10)/F(11)/F(9B) and Xe(2)···F(8)/F(8A)/F(8B) contacts. These arrangements of three primary bonds, three long contacts, and the xenon valence electron lone pair are similar to the distorted octahedral AXY_2Z_3E VSEPR arrangement of α-XeO_2F^+ (vide supra).

The *β*-[XeO_2F][SbF_6] tetramers interact with one another by means of very weak secondary contacts between fluorine ligands on antimony and xenon, which are at or very near the sum of the xenon and fluorine van der Waals radii [Xe(1)···F(12C), 3.562(7) Å; Xe(1)···O/F(4C), 3.673(6) Å; Xe(1)···O/F(3C), 3.681(7) Å; Xe(2)···F(7C)/F(7D)/F(7E), 3.584(5) Å] and approach each xenon such that their trajectories avoid its valence electron lone-pair domain and bisect the O/F−Xe−O/F bond angles. An exception is the Xe(1)···F(6C) [3.409(6) Å] contact, which approaches Xe(1) through the center of the [O/F(1), O/F(2), O/F(3)] face.

(d) [$FO_2XeFXeO_2F$][AsF_6]. The [$FO_2XeFXeO_2F$][AsF_6] structural unit is comprised of well-separated $FO_2XeFXeO_2F^+$ cations and AsF_6^- anions (Figure 3a). When viewed along the *b*-axis, the unit cell of [$FO_2XeFXeO_2F$][AsF_6] shows a two-dimensional layered structure in which double layers of

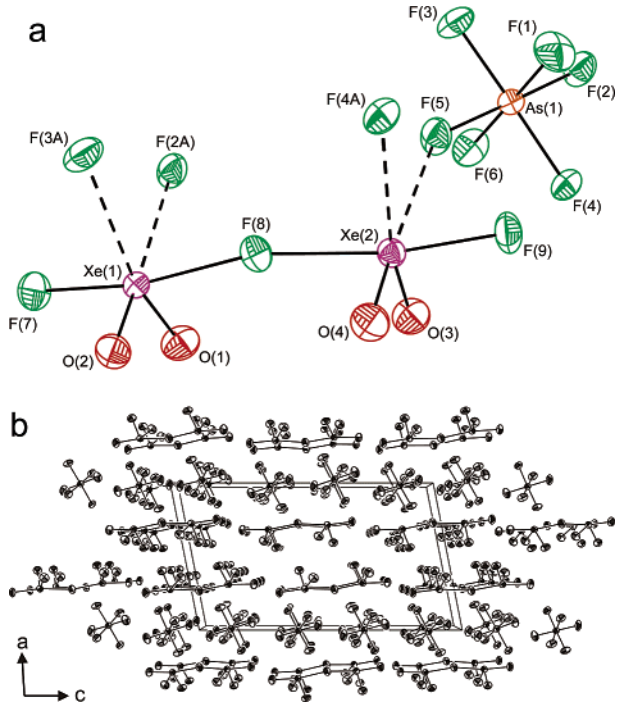

Figure 3. (a) X-ray crystal structure of [FO$_2$XeFXeO$_2$F][AsF$_6$]. Thermal ellipsoids are shown at the 50% probability level. (b) Packing of [FO$_2$XeFXeO$_2$F][AsF$_6$] along the *b*-axis.

FO$_2$XeFXeO$_2$F$^+$ cations are sandwiched between layers of AsF$_6^-$ anions (Figure 3b). The cations, in their double layers, are oriented such that the lone pairs point toward the AsF$_6^-$ anions and the doubly bonded oxygen atoms face each other, much like the packing arrangements observed for the XeO$_2$F$^+$ salts.

The FO$_2$XeFXeO$_2$F$^+$ cation consists of two crystallographically independent XeO$_2$F units bridged by a fluorine atom to give a bent Xe- - -F- - -Xe arrangement. The FO$_2$XeFXeO$_2$F$^+$ cation is one of four known fluorine-bridged noble-gas cations, with the others being F(KrF)$_2^+$,[24] F(XeF)$_2^+$,[25,26] and F(XeF$_5$)$_2^+$.[27] Each F- - -XeO$_2$F moiety approximates a disphenoidal AX$_2$Y$_2$E VSEPR arrangement of the electron lone pair and four bond-pair domains in the xenon valence shell with terminal Xe−F and Xe−O bond lengths that are similar to those of the neutral and cationic xenon(VI) oxide fluorides (vide supra). The terminal Xe−F bond lengths of the FO$_2$XeFXeO$_2$F$^+$ cation are intermediate with respect to those of the XeO$_2$F$^+$ cation in α-[XeO$_2$F][SbF$_6$] and XeO$_2$F$_2$, corresponding to a decrease in charge on xenon and an increase in the Xe−F bond polarity: XeO$_2$F$^+$ > FO$_2$XeFXeO$_2$F$^+$ > XeO$_2$F$_2$.

The FO$_2$XeFXeO$_2$F$^+$ cation is asymmetric about the bridging fluorine atom with Xe- - -F bond lengths of 2.161(3) Å [Xe(1)- - -F(8)] and 2.230(3) Å [Xe(2)- - -F(8)] and has an average torsion angle [O(1/2)−Xe(1)···Xe(2)−O(3/4)] that is essentially 0°, resulting in a cation point symmetry of C_s. In addition to the bridging fluorine common to both xenon centers, each xenon atom of a XeO$_2$F moiety has secondary fluorine bridge contacts from neighboring anions (Table 2). These secondary contacts approach their respective xenon centers such that they avoid the xenon valence electron lone pair and are trans to the equatorial oxygen atoms. The contacting fluorine atoms are nearly coplanar with the triangular planes defined by O(1)−Xe(1)−O(2) and O(3)−Xe(2)−O(4), lying out of these planes by 0.3 Å. Each xenon atom attains a distorted octahedral geometry that is consistent with a monocapped octahedral AXY$_2$Z$_3$E arrangement similar to those inferred from the structures of α- and *β*-[XeO$_2$F][SbF$_6$] and [XeO$_2$F][AsF$_6$] (vide supra). A longer contact, very close to the sum of the fluorine and xenon van der Waals radii [Xe(1)···F(1A), 3.484(4) Å; Xe(2)···F(6A), 3.226(4) Å], also approaches each xenon atom along a trajectory that avoids the electron lone pair on xenon. The approximate positions of the nonbonding electron pair domains on xenon atoms may be inferred from the trajectories of the long contacts and are located between F(1A), F(3A), F(2A), and F(8) and F(6A), F(4A), F(9), and F(8) on Xe(1) and Xe(2), respectively.

The bond valences of the bridging fluorine {0.48 vu [Xe(1)- - -F(8)]; 0.40 vu [Xe(2)- - -F(8)]} are approximately half of the bond valence contribution from the terminal fluorine atoms [F(7) and F(9)] and are consistent with valence bond structures I and III, implying a negligible contribution from valence bond structure II. On average, the secondary fluorine contacts with Xe(2) are shorter than those with Xe(1), giving rise to a somewhat longer Xe(2)- - -F(8) bridge bond and lower bond valence value than that for Xe(1)- - -F(8) and the observed asymmetry of the fluorine bridge.

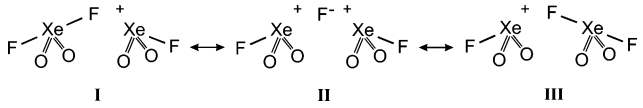

The Xe- - -F- - -Xe bridge angle [166.4(2)°] and bond lengths [2.161(3) and 2.230(3) Å] of FO$_2$XeFXeO$_2$F$^+$ may be compared with those of the fluorine-bridged cations Xe$_2$F$_3^+$ and Xe$_2$F$_{11}^+$. These parameters are very similar to those of Xe$_2$F$_{11}^+$ in its AuF$_6^-$ salt [169.2(2)°; 2.21(1) and 2.26(1) Å].[27] In the [Xe$_2$F$_{11}$]$_2$[NiF$_6$] salt [140.3°; 2.35(1) and 2.21(1) Å],[28] however, the Xe- - -F- - -Xe angle is much smaller and is likely a consequence of stronger cation−anion interactions that result from the higher negative charge on the fluorine ligands of the NiF$_6^{2-}$ anion. This is reflected in the closest Xe···F contacts between the fluorine ligands of the anions and xenon, which are shorter in the NiF$_6^{2-}$ salt (2.49 and 2.53 Å) than in the AuF$_6^-$ salt [2.64(1) and 2.64(1) Å]. The fluorine bridge angles of the xenon(VI) cations are generally larger than, or overlap, the range of Xe- - -F- - -Xe angles [139.8(8)−160.3(3)°] observed in the Xe$_2$F$_3^+$ salts.[25] The fluorine bridge angles of the xenon(II) and xenon(VI) cations are expected to be highly deformable, with the

(24) Lehmann, J. F.; Dixon, D. A.; Schrobilgen, G. J. *Inorg. Chem.* **2001**, *40*, 3002.
(25) Fir, B. A.; Gerken, M.; Pointner, B. E.; Mercier, H. P. A.; Dixon, D. A.; Schrobilgen, G. J. *J. Fluorine* Chem. **2000**, *105*, 159.
(26) Sladky, F. O.; Bulliner, P. A.; Bartlett, N.; DeBoer, B. G.; Zalkin, A. *Chem. Commun.* **1968**, 1048.
(27) Leary, K.; Zalkin, A.; Bartlett, N. *Inorg. Chem.* **1974**, *13*, 775.
(28) Jesih, A.; Lutar, K.; Leban, I.; Žemva, B. *Inorg. Chem.* **1989**, *28*, 2911.

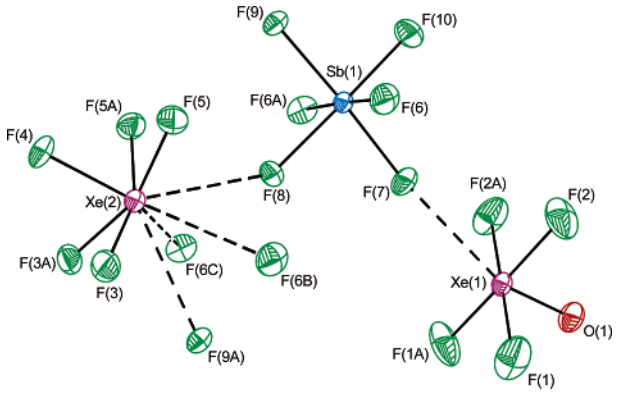

Figure 4. X-ray crystal structure of $[XeF_5][SbF_6]\cdot XeOF_4$. Thermal ellipsoids are shown at the 50% probability level.

larger bridge angles of the xenon(VI) cations likely resulting from strong secondary interactions between their xenon atoms and the fluorine ligands on the anions, whereas such interactions are considerably weaker in the crystal structures of $Xe_2F_3^+$ [25] and $Kr_2F_3^+$ [24] salts and approach the limits of the xenon and fluorine van der Waals radii. The calculated Xe- - -F- - -Xe angle in $FO_2XeFXeO_2F^+$ (142.9−149.7°) is smaller than the experimental value at all levels of theory (see the Geometry Optimizations section), suggesting that the secondary contacts and crystal packing play a role in enlarging this angle. This is consistent with the observation that the contacts enter into the coordination spheres of the xenon atoms of $FO_2XeFXeO_2F^+$ on the side opposite to that in the $Xe_2F_{11}^+$ cation and would be expected to enlarge the Xe- - -F- - -Xe bridge angle.

The F(7)−Xe(1)- - -F(8) [169.7(2)°] and F(9)−Xe(2)- - -F(8) [170.8(2)°] bond angles of the F- - -XeO_2F moieties are bent toward the lone pair of each xenon atom and away from the equatorial Xe−O double-bond domains in a manner similar to that in the structures of XeO_2F_2,[17] $TcO_2F_3\cdot XeO_2F_2$,[18] and $XeO_2(OTeF_5)_2$.[29] There are two secondary fluorine contacts between each xenon atom and two independent AsF_6^- anions on the side opposite to the doubly bonded oxygens. Thus, it is unlikely that the deformation of the F−Xe- - -F angle toward the xenon valence electron lone-pair domain is a consequence of crystal packing (see the Computational Results section for a related discussion). As in the case of the $[XeO_2F][MF_6]$ salts, the longest As−F bonds are those where the fluorine atoms are involved in the shortest contacts to the xenon atoms (Table 2).

(e) $[XeF_5][SbF_6]\cdot XeOF_4$. The crystal structure of $[XeF_5][SbF_6]\cdot XeOF_4$ is comprised of a well-separated $XeOF_4$ molecule and a fluorine-bridged $[XeF_5][SbF_6]$ ion pair (Figure 4). The structure of $XeOF_4$ is a square-based pyramid of approximate C_{4v} symmetry corresponding to an AX_4YE VSEPR arrangement of bond-pair and lone-pair domains. The geometric parameters obtained for $XeOF_4$ in the present crystal structure (Table 2) are in good agreement with the values obtained from previous microwave and electron diffraction structural studies.[14,15] In the current and earlier studies, the O−Xe−F bond angles are also found to be slightly greater than 90°, within $\pm 3\sigma$, implying that the repulsive effect of the doubly bonded oxygen atom is comparable to that of the free valence electron lone pair.

Only one significant secondary contact [Xe(1)···F(7), 2.840(2) Å] occurs between $XeOF_4$ and the SbF_6^- anion. A second, longer contact [Xe(1)···F(10A), 3.564(2) Å] from another SbF_6^- anion is at the limit of the xenon and fluorine van der Waals radii. These contacts approach from beneath the XeF_4 plane of $XeOF_4$ [O−Xe(1)···F(7), 160.80(12)°; O−Xe(1)···F(1A), 142.73(11)°], avoiding the xenon electron lone-pair domain.

The XeF_5^+ cations and SbF_6^- anions are well separated in the structure but interact through fluorine bridges with consequent distortion of the SbF_6^- anion from its regular octahedral geometry (Table 2). The XeF_5^+ cation exhibits a distorted square-based pyramidal geometry corresponding to an AX_5E VSEPR arrangement, which has been well characterized in previous X-ray crystallographic studies[30−34] and requires no further discussion. As in the case of $[XeF_5][MF_6]$ (M = Pt,[30] Ru[32]) and $[XeF_5][AgF_4]$,[34] secondary fluorine bridge contacts between the XeF_5^+ and MF_6^- ions arise from four nearly equidistant MF_6^- anions, which each contribute a long contact from a fluorine atom to the xenon atom [Xe(2)···F(8), 2.592(2) Å; Xe(2)···F(9A), 2.658(2) Å; Xe(2)···F(3B/3C), 3.070(2) Å]. These contacts avoid the electron lone-pair domain of xenon, are approximately coplanar and equidistant from xenon, and are arranged about the C_4-axis of the XeF_5^+ cation in a staggered configuration beneath the equatorial fluorine plane of XeF_5^+ to give a distorted square antiprismatic arrangement (Figure 4).

Thermochemistry: Fluoride Ion Donor Properties of XeO_2F_2 and Stabilities of XeO_2F^+ and $FO_2XeFXeO_2F^+$ Salts. The standard enthalpies and Gibbs free energies for reactions A−I in Table 3 were determined by the application of the appropriate Born−Haber cycles (Figure S1 in the Supporting Information). Electronic structure calculations and established empirical methods[35,36] were used in conjunction with known thermodynamic quantities to estimate $\Delta H°$, $\Delta S°$, and $\Delta G°$. Standard gas-phase entropies, for which no experimental values are available, and gas-phase enthalpy changes were calculated at the MP2/Stutt RLC ECP and MP2/DZVP (values in square brackets) levels. The electronic energies and Gibbs free energies are given in Table S2 in the Supporting Information. The enthalpy changes for the gas-phase fluoride ion transfer reactions between XeO_2F_2 and a Lewis acid were calculated by use of eq 6, where $\Delta H°_{-F^-}$

$$\Delta H°_{F^-} = \Delta H°_{-F^-} + \Delta H°_{+F^-} \qquad (6)$$

is the enthalpy of fluoride ion abstraction from XeO_2F_2 and

(29) Turowsky, L.; Seppelt, K. *Z. Anorg. Allg. Chem.* **1992**, *609*, 153.
(30) Bartlett, N.; Einstein, F.; Stewart, D. F.; Trotter, J. *J. Chem. Soc. A.* **1967**, 1190.
(31) Leary, K.; Templeton, D. H.; Zalkin, A.; Bartlett, N. *Inorg. Chem.* **1973**, *12*, 1726.
(32) Bartlett, N.; Gennis, M.; Gibler, D. D.; Morrell, B. K.; Zalkin, A. *Inorg. Chem.* **1973**, *12*, 1717.
(33) Bartlett, N.; DeBoer, B. G.; Hollander, F. J.; Sladky, F. O.; Templeton, D. H.; Zalkin, A. *Inorg. Chem.* **1974,** *13*, 780.
(34) Lutar, K.; Jesih, A.; Leban, I.; Zemva, B.; Bartlett, N. *Inorg. Chem.* **1989**, *28*, 3467.

Table 3. Values of $\Delta H°$, $\Delta S°$, and $\Delta G°$ Calculated for Reactions of XeO_2F_2 with AsF_5, SbF_5, and Sb_2F_{10} and for the Decompositions of XeO_2F^+ Salts

	$\Delta H°$,[a,b] kJ mol^{-1}	$\Delta S°$,[c] J mol^{-1} K^{-1}	$\Delta G°$, [d,b] kJ mol^{-1}
Formation of XeO_2F^+ and $FO_2XeFXeO_2F^+$ Salts			
(A) $XeO_2F_2(s) + AsF_5(g) \rightarrow [XeO_2F][AsF_6](s)$	−11.5 [−30.9]	−562.2	156.1 [136.7]
(B) $XeO_2F_2(s) + SbF_5(l) \rightarrow [XeO_2F][SbF_6](s)$	−33.1 [−65.1]	−328.5	64.8 [32.8]
(C) $XeO_2F_2(s) + 2SbF_5(l) \rightarrow [XeO_2F][Sb_2F_{11}](s)$	−12.6 [−54.7]	−453.2	122.9 [80.4]
(D) $2XeO_2F_2(s) + AsF_5(g) \rightarrow [FO_2XeFXeO_2F][AsF_6](s)$	−25.9 [−43.5][e]	−766.0	202.4 [184.9][e]
(E) $2XeO_2F_2(s) + SbF_5(l) \rightarrow [FO_2XeFXeO_2F][SbF_6](s)$	−49.2 [−79.4][e]	−530.0	108.8 [78.6][e]
(F) $2[XeO_2F][AsF_6](s) \rightarrow [FO_2XeFXeO_2F][AsF_6](s) + AsF_5(g)$	−3.0 [18.2][e]	358.4	−103.8 [−88.7][e]
Decompositions of XeO_2F^+ Salts			
(G) $[XeO_2F][AsF_6](s) \rightarrow [XeF][AsF_6](s) + O_2(g)$	−369.3 [−473.1]	179.4	−422.8 [−526.6]
(H) $[XeO_2F][SbF_6](s) \rightarrow [XeF][SbF_6](s) + O_2(g)$	−366.3 [−470.1]	181.8	−420.5 [−524.3]
(I) $[XeO_2F][Sb_2F_{11}](s) \rightarrow [XeF][Sb_2F_{11}](s) + O_2(g)$	−359.7 [−463.5]	181.8	−413.9 [−517.7]

[a] Calculated from eq 11 or 12. [b] MP2/Stutt RLC and MP2/DZVP (values in square brackets). [c] The explicit expressions for calculation of the standard entropies from experimental values (see text) are given in Table S3 in the Supporting Information. [d] $\Delta G° = \Delta H° - T\Delta S°$. [e] The values are for the crystallographic symmetry of $FO_2XeFXeO_2F^+$ (C_s) and differ by ±0.1 kJ mol^{-1} with respect to those for the energy-minimized geometry having C_1 symmetry.

$\Delta H°_{+F^-}$ is the enthalpy of fluoride ion attachment to MF_5 (M = As, Sb) and Sb_2F_{10}, which are compared with the MP2/PDZ[37] and NDLFT[38] values (Table 4). The gas-phase enthalpies and Gibbs free energies (195.15 and 298.15 K) for the formation of the fluorine-bridged $FO_2XeFXeO_2F^+$ cation from XeO_2F_2 and XeO_2F^+ (eq 7) and for the decomposition of the XeO_2F^+ cation (eq 8) were also calculated from the MP2 energies. The values for $XeO_2{}^+F^+$ and XeO_2F_2 are comparable and the decomposition pathway for XeO_2F^+ is consistent with the known decomposition pathway for XeO_2F_2 to XeF_2 and O_2 (eq 9).[39]

$$XeO_2F^+(g) + XeO_2F_2(g) \rightarrow FO_2XeFXeO_2F^+(g) \quad (7)$$

$$\Delta H°_{bridge} = -97.7\,[-119.6]\ \text{kJ mol}^{-1}$$

$$\Delta G°^{298}_{bridge} = -56.6\,[-78.6]\ \text{kJ mol}^{-1}$$

$$\Delta G°^{195}_{bridge} = -96.1\,[-94.9]\ \text{kJ mol}^{-1}$$

$$XeO_2F^+(g) \rightarrow XeF^+(g) + O_2(g) \quad (8)$$

$$\Delta H°_{decomp} = -341.5\,[-455.8]\ \text{kJ mol}^{-1}$$

$$\Delta G°^{298}_{decomp} = -379.3\,[-493.0]\ \text{kJ mol}^{-1}$$

$$\Delta G°^{195}_{decomp} = -375.5\,[-479.1]\ \text{kJ mol}^{-1}$$

$$XeO_2F_2(g) \rightarrow XeF_2(g) + O_2(g) \quad (9)$$

$$\Delta H°_{decomp} = -354.5\,[-479.8]\ \text{kJ mol}^{-1}$$

$$\Delta G°^{298}_{decomp} = -393.4\,[-518.2]\ \text{kJ mol}^{-1}$$

$$\Delta G°^{195}_{decomp} = -378.7\,[-503.7]\ \text{kJ mol}^{-1}$$

The enthalpies of sublimation and vaporization of XeO_2F_2 and SbF_5, respectively, are required to complete Born−Haber cycles (Figure S1) for reactions A−E in Table 3. The value used for $\Delta H°_{sub}(XeO_2F_2)(s)$ (53.15 kJ mol^{-1}) was obtained from low-energy electron impact ionization mass spectrometry.[40] Although the enthalpy of vaporization term ($\Delta H°_{vap}$) of AsF_5 is zero because it is a gas under standard conditions, $\Delta H°_{vap}$ must be accounted for in reactions involving SbF_5, a viscous polymeric liquid at ambient temperature. The determination of $\Delta H°_{vap}$ for $(SbF_5)_m$ (m = 1 and 2) is complicated by the polymeric nature of liquid SbF_5 and the predominance of the $(SbF_5)_3$ trimer in the gas phase at ambient temperature.[41] The enthalpy of vaporization for monomeric SbF_5 has been estimated to be 30.9 kJ mol^{-1} [42] from the enthalpy of vaporization for $(SbF_5)_3$ (43.4 kJ mol^{-1})[43] and the dissociation energy reported for $^1/_4(SbF_5)_4$ to SbF_5 (18.5 kJ mol^{-1}).[44] Assuming the heat of dissociation of $(SbF_5)_4$ to $2Sb_2F_{10}$ is close to thermally neutral, provided the numbers of Sb- - -F- - -Sb bridges broken and reformed are equal, a reasonable estimate for the enthalpy of vaporization for Sb_2F_{10} is given by $^2/_3\Delta H°_{vap}((SbF_5)_3)$ = 28.9 kJ mol^{-1}.

Table 4. Standard Enthalpies of Reaction Determined for Gas-Phase Fluoride Ion Transfer Reactions Involving XeO_2F_2, AsF_5, SbF_5, and Sb_2F_{10}

	$\Delta H°_{\pm F^-}$, kJ mol^{-1}
Enthalpy of F^- Detachment, $\Delta H°_{-F^-}$	
$XeO_2F_2(g) \rightarrow XeO_2F^+(g) + F^-(g)$	920.7 [941.1]
Enthalpy of F^- Attachment, $\Delta H°_{+F^-}$	
$AsF_5(g) + F^-(g) \rightarrow AsF_6{}^-(g)$	−451.3 [−491.1] (−443,[b] 440[c])
$SbF_5(g) + F^-(g) \rightarrow SbF_6{}^-(g)$	−510.3 [−562.7] (−503,[b] 473[c])
$Sb_2F_{10}(g) + F^-(g) \rightarrow Sb_2F_{11}{}^-(g)$	−547.3 [−610.2] (531[c])

[a] Calculated by use of the MP2/Stutt RLC ECP and MP2/DZVP (values in square brackets) methods. [b] MP2/PDZ.[37] [c] NLDFT.[38]

The lattice enthalpies of the XeO_2F^+ and $FO_2XeFXeO_2F^+$ salts (Table 5) were estimated by use of the empirical volume-based method[45] recently generalized by Jenkins et

(35) Jenkins, H. D. B.; Roobottom, H. K.; Passmore, J.; Glasser, L. *Inorg. Chem.* **1999**, *38*, 3609.
(36) Jenkins, H. D. B.; Glasser, L. *Inorg. Chem.* **2003**, *42*, 8702.
(37) Christe, K. O.; Dixon, D. A.; McLemore, D.; Wilson, W. W.; Sheehy, J. A.; Boatz, J. A. *J. Fluorine Chem.* **2000**, *101*, 151.
(38) Christe, K. O.; Dixon, D. A. Presented at the 16th Winter Fluorine Conference, St. Petersburg, FL, Jan 12−17, 2003.
(39) Huston, J. L. *J. Phys. Chem.* **1967**, *71*, 3339.
(40) Zelenov, V. V.; Aparina, E. V.; Loboda, A. V.; Kukui, A. S.; Dodonov, A. F. *Eur. J. Mass Spectrom.* **2002**, *8*, 233.
(41) Brunvoll, J.; Ishchenko, A. A.; Myakshin, I. N.; Romanov, G. V.; Spiridonov, V. P.; Strand, T. G.; Sukhoverkhov, V. F. *Acta Chem. Scand.* **1980**, *A34*, 733.
(42) Bougon, R.; Bui Huy, T.; Burgess, J.; Christe, K. O.; Peacock, R. D. *J. Fluorine Chem.* **1982**, *19*, 263.
(43) Shair, R. C.; Schurig, W. F. *Ind. Eng. Chem.* **1951**, *43*, 1624.
(44) Fawcett, J.; Holloway, J. H.; Peacock, R. D.; Russell, D. K. *J. Fluorine Chem.* **1982**, *20*, 9.

Table 5. Estimated[a] Formula Unit Volumes, Standard Lattice Enthalpies, and Standard Lattice Entropies of Salts Containing the XeO_2F^+, $FO_2XeFXeO_2F^+$, and XeF^+ Cations

salt	V_m,[a] nm^3	ΔH_L°,[b] kJ mol^{-1}	S°,[c] J mol^{-1} K^{-1}
$[XeO_2F][AsF_6]$	0.1679	−534.0	243.3
α-$[XeO_2F][SbF_6]$	0.1759	−527.5	254.2
β-$[XeO_2F][SbF_6]$	0.1766	−527.5	255.2
$[XeO_2F][Sb_2F_{11}]$	0.2794[d]	−467.6	395.0
$[FO_2XeFXeO_2F][AsF_6]$	0.2520	−480.2	357.7
$[FO_2XeFXeO_2F][SbF_6]$	0.2621[d]	−475.4	371.4
$[XeF][AsF_6]$	0.1490	−551.3	217.6
$[XeF][SbF_6]$	0.1590	−541.8	231.3
$[XeF][Sb_2F_{11}]$	0.2622	−475.3	371.6

[a] The formula unit volumes, V_m, were obtained from their crystallographic unit cells. [b] The lattice enthalpies (ΔH_L°) were calculated as described in ref 35. [c] The standard entropies were calculated as described in ref 36. [d] Values were estimated assuming that cation and anion volume additivity applies (ref 35) by means of the following relationships: $V_m([XeO_2F][Sb_2F_{11}]) = V_m([XeO_2F][SbF_6]) + V_m([XeF][Sb_2F_{11}]) - V_m([XeF][SbF_6])$; $V_m([FO_2XeFXeO_2F][SbF_6]) = V_m([FO_2XeFXeO_2F][AsF_6]) + V_m([XeF][SbF_6]) - V_m([XeF][AsF_6])$.

al.[35,36] in eq 10, where ΔH_L° is the lattice enthalpy, R is the

$$\Delta H_L^\circ = 2I\left(\frac{\alpha}{\sqrt[3]{V_m}} + \beta\right) + nRT \qquad (10)$$

gas constant, and the constants $I = 1$ (the ionicity of the salt), $\alpha = 117.3$ kJ mol^{-1} nm, $\beta = 51.9$ kJ mol^{-1}, and $n = 2$ depend on the nature of the salt.[35] The net enthalpies of reaction calculated for the formation of the XeO_2F^+ and $FO_2XeFXeO_2F^+$ salts for the reactions of XeO_2F_2 with AsF_5 and $(SbF_5)_n$ ($n = 1$ and 2; eq 11) and the decompositions of XeO_2F^+ salts to XeF^+ salts (eq 12) are summarized in Table 3.

$$\Delta H^\circ = \Delta H_{vap}^\circ + \Delta H_{F^-}^\circ + \Delta H_{decomp}^\circ - \Delta H_L^\circ \qquad (11)$$

$$\Delta H^\circ = \Delta H_{decomp}^\circ + \Delta H_L^\circ[XeF^+ \text{ salt}] - \Delta H_L^\circ[XeO_2F^+ \text{ salt}] \qquad (12)$$

Standard lattice entropies of the XeO_2F^+, XeF^+, and $FO_2XeFXeO_2F^+$ salts (Table 5) have been estimated from their unit volumes (eq 13),[36] where $k = 1360$ J K^{-1} mol^{-1} nm^{-3}

$$S^\circ([\text{cation}][\text{anion}]) = kV_m + c \qquad (13)$$

and $c = 15$ J K^{-1} mol^{-1}. When coupled with the known standard entropies of XeO_2F_2(s) (317.0[46] and 319.4[47] J mol^{-1} K^{-1}), AsF_5(g) (487.3 J mol^{-1} K^{-1}),[48] SbF_5(l) (265 J mol^{-1} K^{-1}),[49] and O_2(g) (205.14 J mol^{-1} K^{-1}),[50] this allows ΔS° and ΔG° to be calculated for reactions A−I in Table 5.

The standard enthalpies of reaction leading to the formation of $[XeO_2F][MF_6]$, $[XeO_2F][Sb_2F_{11}]$, and $[FO_2XeFXeO_2F][AsF_6]$ from MF_5 and XeO_2F_2 are all mildly exothermic (reactions A−E in Table 3), with negative standard entropies that result in standard Gibbs free energies that are significantly positive. It may be concluded that these salts, once isolated from HF solvent at low temperature, derive their room-temperature stabilities with respect to dissociation from kinetic factors and that their formation is favored at lower temperatures. The AsF_6^- salts are less stable than the SbF_6^- salts, reflecting the higher fluoride ion affinity of SbF_5 and the higher entropy contribution of gaseous AsF_5. The $[FO_2XeFXeO_2F][AsF_6]$ salt is less stable than $[XeO_2F][AsF_6]$ primarily because of its lower lattice energy and the additional energy required to sublime 2 mol of XeO_2F_2. The negative ΔG° value for reaction F in Table 3 is consistent with the dissociation of 2 mol of $[XeO_2F][AsF_6]$ to $[FO_2XeFXeO_2F][AsF_6]$ and AsF_5 under dynamic vacuum has been observed in the present and previous[9] studies, which also reported a dissociation pressure of 7 Torr at 23 °C for $[XeO_2F][AsF_6]$. Previous studies have shown that SbF_5 solutions of $[XeO_2F][Sb_2F_{11}]$ rapidly decompose at room temperature, yielding XeF^+ and O_2,[2,5] and that solid $[XeO_2F][Sb_2F_{11}]$ decomposes over a period of several months at room temperature,[4] which was confirmed in the present study. The decompositions of the MF_6^- and $Sb_2F_{11}^-$ salts of XeO_2F^+ to their corresponding XeF^+ salts are predicted to be highly exothermic and spontaneous for reactions G−I (Table 3) at all temperatures. The large negative ΔH° and ΔG° values corresponding to the decomposition are very similar from salt to salt because they are dominated by the large gas-phase enthalpy of decomposition for XeO_2F^+ (eq 8). Moreover, the standard entropy of O_2(g) favors spontaneity, but the small lattice energy and lattice entropy changes upon XeF^+ salt formation have little effect on ΔH° and ΔG°. Dissolution of the XeO_2F^+ salts in SbF_5 and replacement of the lattice energy contributions by solvated XeO_2F^+ and XeF^+ cations and by XeO_2F^+- - -$Sb_nF_{5n-1}^-$ and XeF^+- - -$Sb_nF_{5n-1}^-$ ion-pair interactions more closely approximate gas-phase conditions so that decompositions in SbF_5 solvent are expected to be more exothermic than those of the solid XeO_2F^+ salts.

Although reactions A−E (Table 3) are not spontaneous under standard conditions, their negative ΔS° values indicate that these reactions will tend toward spontaneity at the lower temperatures at which $[XeO_2F][MF_6]$ and $[FO_2XeFXeO_2F][AsF_6]$ have proven to be isolable from anhydrous HF. The positive enthalpies of these reactions and their contributions to the Gibbs free energies are diminished by HF solvation of the reactants and products. The degree to which XeO_2F^+ is stabilized and reaction spontaneity is promoted by HF solvation of XeO_2F^+ has been assessed by calculating the BSSE-corrected[51,52] enthalpies and Gibbs free energies at the MP2/Stutt RLC ECP level for five successive solvation steps, leading to $XeO_2F^+ \cdot x$HF ($x = 1-5$; eq S1) at 298.15 and 195.15 K, and is dealt with in the Supporting Information.

Computational Results: Geometries and Bonding in XeO_2L_2, XeO_2L^+, IO_2F, TeO_2F^-, and $FO_2XeFXeO_2F^+$ (L

(45) Mallouk, T. E.; Rosenthal, G. L.; Müller, G.; Brusasco, R.; Bartlett, N. *Inorg. Chem.* **1984**, *23*, 3167.
(46) Kudchadker, S. A.; Kudchadker, A. P. *Proc. Ind. Acad. Sci. A* **1971**, *73*, 261.
(47) Baran, E. J. *Ind. J. Pure Appl. Phys.* **1977**, *15*, 450.
(48) O'Hare, P. A. G. *J. Chem. Thermodyn.* **1993**, *25*, 391.
(49) Nagarajan, G. *Bull. Soc. Chim. Belg.* **1962**, *71*, 324.
(50) Wagman, D. D.; Evans, W. H.; Parker, V. B.; Schumm, R. H.; Halow, I.; Bailey, S. M.; Churney, K. L.; Nutall, R. L. *J. Phys. Chem. Ref. Data, Suppl.* 2, **1982**, *11*, 37.
(51) Simon, S.; Duran, M.; Dannenberg, J. J. *J. Chem. Phys.* **1996**, *105*, 11024.
(52) Boys, S. F.; Bernardi, F. *Mol. Phys.* **1970**, *19*, 553.

= F, $OTeF_5$). The known, structurally related $OTeF_5$ derivatives $XeO_2(OTeF_5)_2$[29] and $XeO_2(OTeF_5)^+$ [53] were also studied and are mainly dealt with in the Supporting Information.

(a) Geometry Optimizations. The gas-phase geometries of XeO_2F_2 (C_{2v}), XeO_2F^+ (C_s), IO_2F (C_s), TeO_2F^- (C_s), and $FO_2XeFXeO_2F^+$ (C_1) were fully optimized at HF, SVWN, and MP2 levels of theory using DZVP and Stuttgart ECP basis sets, and those of $XeO_2(OTeF_5)^+$ (C_1) and $XeO_2(OTeF_5)_2$ (C_1) were optimized at HF and SVWN levels using Stuttgart ECP basis sets. All calculations resulted in stationary points, with all frequencies real. The calculated frequencies of XeO_2F_2, XeO_2F^+, and $FO_2XeFXeO_2F^+$ are in agreement with experimental values and their previous assignments (Tables S4−S6). Calculated geometric parameters are listed in Tables 6 and S7 along with experimental parameters when available, and calculated geometries are provided in Figure 5. The best agreement with the experiment was obtained using the Stuttgart basis set. Only these values are reported in Table 6 and are referred to in the present discussion.

(i) XeO_2F_2 and $XeO_2(OTeF_5)_2$. Although there are secondary oxygen or fluorine bridge contacts within the solid-state layered structures of XeO_2F_2[17] and $XeO_2F_2{\cdot}TcO_2F_3$,[18] the experimental AX_2Y_2E geometries of the XeO_2F_2 molecules in these crystal structures are well reproduced by the calculations. Secondary contacts among $XeO_2(OTeF_5)_2$ molecules in the crystal structure[29] are significantly weaker than those in the solid-state structures of XeO_2F_2[17] and $XeO_2F_2{\cdot}TcO_2F_3$.[18] This is reflected in the better agreement between the geometrical parameters calculated at the HF/Stutt RLC ECP level and the values obtained from the X-ray structure.

Among the key experimental structural features present in the solid-state structures of XeO_2F_2 and $XeO_2(OTeF_5)_2$ that are reproduced by the calculated geometries are the axial F−Xe−F [calcd 166.9−174.6°; exptl 174.7(4)[17] and 175.7(6)°[18]] and axial O−Xe−O [calcd 156.0−168.6°; exptl 164.1(2)°] angles of XeO_2F_2 and $XeO_2(OTeF_5)_2$, which are bent toward the lone pair on xenon instead of away from it, as in AX_4E-type molecules[8] (see NBO and ELF analyses below). The equatorial O−Xe−O angles of XeO_2F_2 [calcd 108.1−109.3°; exptl 105.7(3)[17] and 105.6(3)°[18]] and $XeO_2(OTeF_5)_2$ [calcd 108.2−108.9°; exptl 105.6(2)°] are more open for the calculated geometries.

The tendency for XeO_2F_2 to form the layered structures observed in its crystal structure[17] is apparent from the lowest unoccupied molecular orbital (LUMO) (see Figure 6). The large lobes on xenon are directed toward and can overlap with the lobes on the oxygen atoms of two neighboring XeO_2F_2 molecules, resulting in a weak bonding interaction. The situation differs for $XeO_2F_2{\cdot}TcO_2F_3$, where the secondary contacts are with neighboring fluorine atoms, one from a XeO_2F_2 molecule and two from adjacent layers of TcO_2F_3 molecules.

(ii) XeO_2F^+, IO_2F, and TeO_2F^-. The title species are isoelectronic, and although they interact in the solid state by means of secondary contacts between the coordinately unsaturated central heavy atom and fluorine/oxygen ligand electron lone pairs of neighboring ions or molecules, their

Table 6. Experimental and Calculated Geometrical Parameters (Å and deg) in XeO_2F_2 (C_{2v}), XeO_2F^+ (C_s), IO_2F (C_s), TeO_2F^- (C_s), and $FO_2XeFXeO_2F^+$ (C_1)

XeO_2F_2

		Stuttgart RLC ECP		
	exptl[a]	HF	SVWN	MP2
Xe−O	1.714(4)	1.720	1.779	1.737
Xe−F	1.899(3)	1.881	1.977	1.968
O−Xe−O	105.7(3)	109.3	108.1	108.3
O−Xe−F	91.6(1)	91.6	93.8	93.7
F−Xe−F	174.7(4)	174.6	166.9	167.3

XeO_2F^+

		Stuttgart RLC ECP		
	exptl[b]	HF	SVWN	MP2
Xe−O(1)	1.740(3)	1.703	1.777	1.729
Xe−O(2)	1.726(3)	1.703	1.777	1.729
Xe−F(1)	1.849(2)	1.806	1.922	1.919
O(1)−Xe−O(2)	105.0(2)	109.3	109.7	110.3
O(1)−Xe−F(1)	95.7(1)	100.5	101.6	100.5
O(2)−Xe−F(1)	98.2(1)	100.5	101.6	100.5

IO_2F[d]

		Stuttgart RLC ECP		
	exptl[c]	HF	SVWN	MP2
I−O (b)	1.805(6)	1.753	1.816	1.786
I−O (t)	1.773(6)			
I−F	1.903(5)	1.873	1.981	1.981
O−I−O (t,b)	99.2(3)	110.3	110.7	111.3
O−I−F (b)	94.6(2)	99.9	100.9	100.4
O−I−F (t)	90.7(2)			

TeO_2F^-[d]

		Stuttgart RLC ECP		
	exptl[e]	HF	SVWN	MP2
Te−O (t)	1.807(4)	1.797	1.850	1.839
Te−O (b)	1.904(10), 2.080(6)			
Te−F	2.095(8)	1.930	2.023	2.019
O−Te−O (t,b)	91.4(1.9), 99.7(1.3)	110.1	109.8	110.6
O−Te−O (b,b)	89.5(9)			
O−Te−F (b)	85.0(1.7), 173.2(1.7)	99.4	100.2	100.1
O−Te−F (t)	87.4(8)			

$FO_2XeFXeO_2F^+$

		Stuttgart RLC ECP		
	exptl[b]	HF	SVWN	MP2
Xe(1)−F(1)	1.872(3)	1.820	1.929	1.924
Xe(1)−F(3)	2.230(3)	2.194	2.240	2.265
Xe(1)−O(1)	1.715(4)	1.709	1.773	1.730
Xe(1)−O(2)	1.721(4)	1.709	1.774	1.730
Xe(2)−F(2)	1.870(4)	1.820	1.929	1.924
Xe(2)−F(3)	2.161(3)	2.194	2.240	2.265
Xe(2)−O(3)	1.719(4)	1.709	1.774	1.730
Xe(2)−O(4)	1.719(4)	1.709	1.773	1.730
O(1)−Xe(1)−F(1)	96.0(2)	96.2	97.8	98.0
O(1)−Xe(1)−F(3)	89.9(2)	88.4	91.0	92.3
O(1)−Xe(1)−O(2)	105.8(2)	109.0	108.8	108.6
O(2)−Xe(1)−F(3)	89.8(2)	88.7	90.8	91.5
F(1)−Xe(1)−O(2)	95.4(2)	96.2	97.7	97.8
F(1)−Xe(1)−F(3)	170.8(2)	171.8	165.0	163.0
Xe(1)−F(3)−Xe(2)	166.4(2)	149.7	144.1	142.9
F(2)−Xe(2)−O(3)	95.2(2)	96.2	97.7	97.8
F(2)−Xe(2)−O(4)	95.6(2)	96.2	97.8	98.0
F(2)−Xe(2)−F(3)	169.7(2)	171.8	165.0	163.0
O(3)−Xe(2)−O(4)	105.8(2)	109.0	108.8	108.6
O(3)−Xe(2)−F(3)	91.1(2)	88.7	90.8	91.5
O(4)−Xe(2)−F(3)	90.6(2)	88.4	91.0	92.3

[a] Reference 16. [b] This work; from α-$[XeO_2F][SbF_6]$. [c] Reference 21. [d] The symbols t and b denote terminal and bridging oxygens, respectively. [e] Reference 22.

(53) Syvret, R. G.; Mitchell, K. M.; Sanders, J. C. P.; Schrobilgen, G. J. *Inorg. Chem.* **1992**, *31*, 3381.

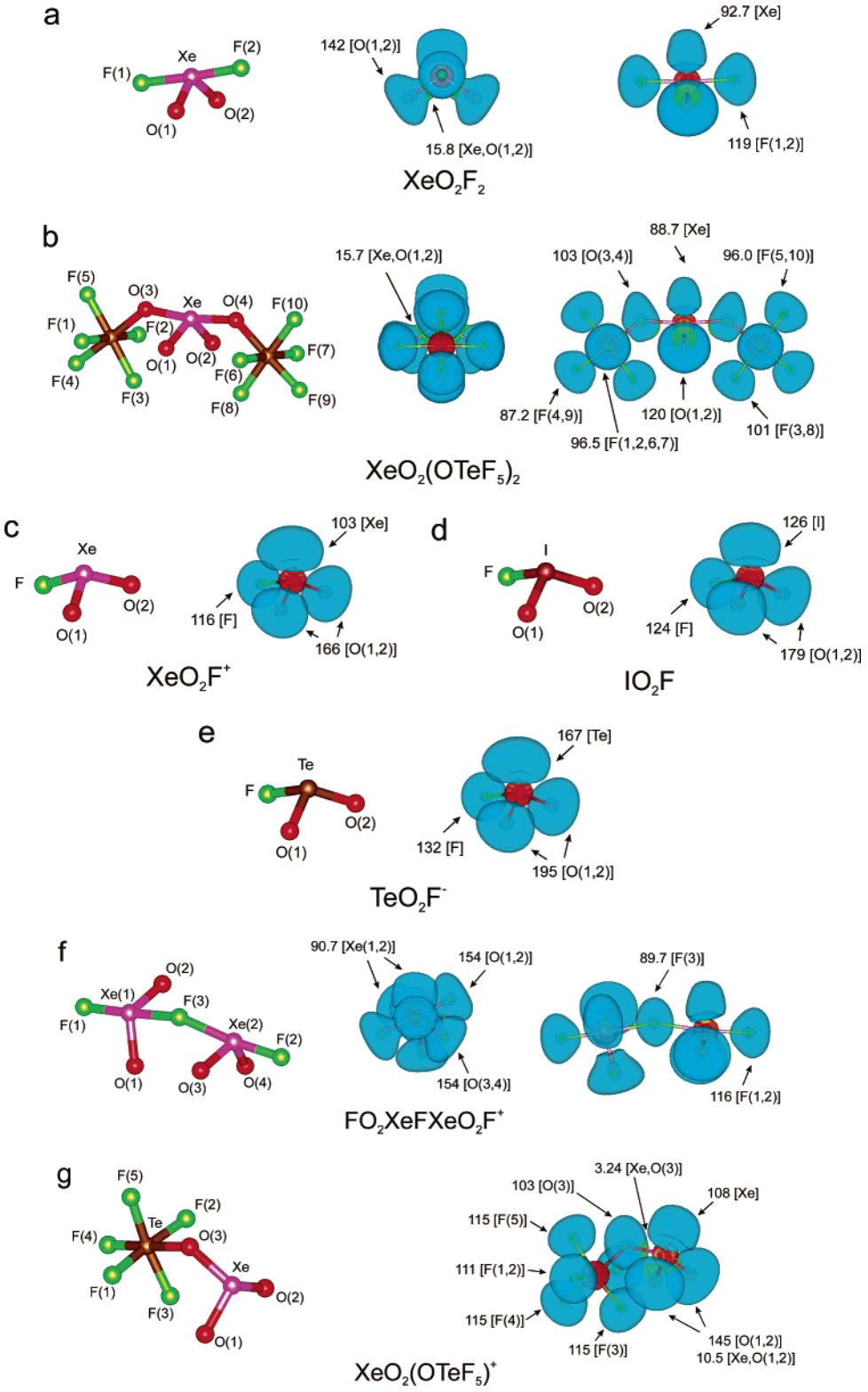

Figure 5. Calculated geometries (left; see Tables 6 and S7 for bond lengths and angles) and ELF isosurface plots (right) at the 0.5 contour level for (a) XeO_2F_2 viewed along O−Xe−O (center) and F−Xe−F (right), (b) $XeO_2(OTeF_5)_2$ viewed along O(1)−Xe−O(2) (center) and O(3)−Xe−O(4) (right), (c) XeO_2F^+, (d) IO_2F, (e) TeO_2F^-, and (f) $FO_2XeFXeO_2F^+$ viewed along F−Xe−F (center) and O−Xe−O (right), and (g) $XeO_2(OTeF_5)^+$ viewed along O(1)−Xe−O(2), at the HF/DZVP level. Color scheme: light blue, monosynaptic (lone-pair) basin, $V(X_i)$; light green, bisynaptic (bond) basin; $V(E,X_i)$; red, core basin. Values shown are for the basin volumes (arbitrary units) of $V(X_i)$ and $V(E,X_i)$.

trigonal-pyramidal geometries as well as the lengthening with increasing net negative charge observed for the experimental bond lengths are well reproduced by the calculations. The XeO_2F^+ cation forms long contacts to the fluorine atoms of the MF_6^- anion (see the X-ray Crystal Structures section), whereas association in the solid-state structures of IO_2F and TeO_2F^- is primarily the result of oxygen bridging. Iodyl fluoride forms infinite chains[21] and TeO_2F^- is a cyclic trimer,

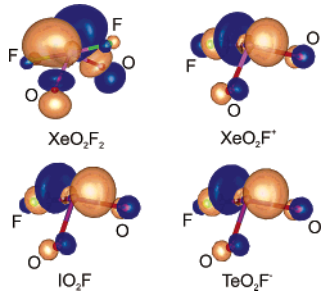

Figure 6. LUMO orbitals at the 0.08 contour value for XeO_2F_2, XeO_2F^+, IO_2F, and TeO_2F^- at the HF/DZVP level.

$[Te_3O_6F_3]^{3-}$,[22] as a result of contacts between the heavy atoms and oxygen atoms of neighboring molecules/anions. These weak, associative Lewis acid−base interactions may result from the overlap of the unoccupied orbitals with the oxygen lone-pair MO orbitals of neighboring molecules/anions (Figure 6). Although the LUMO of XeO_2F^+ (Figure 6) is very similar to those of IO_2F and TeO_2F^-, the net positive charge on XeO_2F^+ leads to long ionic contacts with MF_6^- anions instead of the more covalent LUMO−lone pair MO interactions seen for neutral IO_2F and anionic TeO_2F^-.

(iii) $FO_2XeFXeO_2F^+$. A preliminary optimization was attempted using the experimental symmetry (C_s), which gave rise to an O−Xe···Xe−O torsion angle of 0°. The calculated frequencies revealed one imaginary frequency, showing the geometry corresponding to a first-order transition state. A second geometry optimization starting from the geometry suggested by the imaginary frequency led to a true minimum having C_1 symmetry. The bond lengths and angles were almost the same as those for C_s symmetry with a symmetrical Xe- - -F- - -Xe bridge, but the O−Xe···Xe−O torsion angle was +34.6 to −70.4°, depending on the level of theory used. This indicates that both terminal FO_2Xe groups are relatively free to rotate with respect to the central bridging fluorine atom [F(3), which has long, weak bonds (calcd 2.194−2.314 Å) and is supported by the low frequency calculated for the corresponding torsional mode (19−34 cm^{-1}; Table S6)]. Thus, the torsion angle, which is 0.4° in the experimental structure, is likely determined by crystal packing. The best fit for the bond lengths is given by HF/Stutt RLC ECP, although the bond lengths are systematically shorter when compared with the experimental values, where the anion−cation interactions in the solid-state structures are expected to result in the lengthening of the Xe−O and Xe−F bonds. The Xe- - -F- - -Xe bridge angle is calculated to be ca. 20° smaller than that in the crystal structure and is also likely influenced by crystal packing and the deformability of this angle (calcd δ(Xe- - -F- - -Xe), 178−250 cm^{-1}; Table S6).

(b) Natural Bond Orbital (NBO) and Electron Localization Function (ELF) Analyses. The NBO[54−57] analyses were carried out for optimized gas-phase structures of XeO_2F_2, XeO_2F^+, IO_2F, TeO_2F^-, and $FO_2XeFXeO_2F^+$ using the MP2/Stutt RLC ECP method. For XeO_2F_2, XeO_2F^+, IO_2F, and TeO_2F^-, nine different natural Lewis structures (six for $FO_2XeFXeO_2F^+$) were considered, and the three dominant Lewis structures for each species were arrived at using the criterion of lowest percentage of non-Lewis electrons calculated from the total electron count. The total and ionic natural valencies were also calculated using the Natural Resonance Theory (NRT).[58−60] The NBO and NRT results are given in Tables7 and S8 and S9. The ELF[61−63] analyses were performed at the HF/DZVP level using MP2 geometries, and relevant information is given in Figure 5 (for details, see the Supporting Information). In the case of the larger systems, $XeO_2(OTeF_5)^+$ and $XeO_2(OTeF_5)_2$, Stutt RLC ECP basis sets were used for the ELF analyses (see the discussion and Table S10).

(i) XeO_2F_2. The MP2 NBO analysis gives natural charges of 3.00 and 2.91 for Xe in XeO_2F_2 and $XeO_2(OTeF_5)_2$, respectively. These charges, which are approximately the average of the formal charge 0 (covalent model) and formal oxidation number 6 (ionic model) for Xe in both molecules, are in accordance with the natural charges for O (−0.90) and F (−0.60) in XeO_2F_2, which are also about half of their respective oxidation numbers, and indicate that the bonds in XeO_2F_2 are semi-ionic. The NBO natural charges on the terminal (−0.86) and bridging (−1.11) O atoms in $XeO_2(OTeF_5)_2$ are also consistent with strong polar contributions to the bonding.

The ELF analysis of XeO_2F_2 shows that the bisynaptic bond basins V(Xe,O_i) (Table S10), with electron populations of 1.33 and basin volumes of 15.8, have substantial contributions from the Xe core basin (28%). Although high basin populations have sometimes been attributed to high formal covalent bond orders, this correlation has been questioned, and it has been shown to be unreliable for polar bonds involving heavy elements.[64] At the ELF contour value of 0.50, these bond basins, which are located between xenon and oxygen atoms but are somewhat closer to oxygen (Figure 5), indicate polar Xe−O double bonds. In contrast, there are no bond basins between Xe and F at the 0.50 contour level, in accordance with the low Xe−F natural bond orders (0.30−0.35) obtained from the NBO analyses (Table S9). The nonbonding "lone pair" V_2(Xe) basin is shown to be more diffuse in the O−Xe−O equatorial plane than along the F−Xe−F axial plane, which results in the observed and calculated bending of the axial fluorine atoms away from the oxygen atoms, which is consistent with the Robinson−

(54) Reed, A. E.; Weinstock, R. B.; Weinhold, F. *J. Chem. Phys.* **1985**, *83*, 735.
(55) Reed, A. E.; Curtiss, L. A.; Weinhold, F. *Chem. Rev.* **1988**, *88*, 899.
(56) Glendening, E. D.; Reed, A. E.; Carpenter, J. E.; Weinhold, F. *NBO*, version 3.1; Gaussian, Inc.: Pittsburgh, PA, 1990.
(57) Glendening, E. D.; Badenhoop, J. K.; Reed, A. E.; Carpenter, J. E.; Bohmann, C. M.; Morales, C. M.; Weinhold, F. *NBO*, version 5.0; Theoretical Chemistry Institute, University of Wisconsin: Madison, WI, 2001.
(58) Glendening, E. D.; Weinhold, F. *J. Comput. Chem.* **1998**, *19*, 593.
(59) Glendening, E. D.; Weinhold, F. *J. Comput. Chem.* **1998**, *19*, 610.
(60) Glendening, E. D.; Badenhoop, J. K.; Weinhold, F. *J. Comput. Chem.* **1998**, *19*, 628.
(61) Noury, S.; Krokidis, X.; Fuster, F.; Silvi, B. *TopMod package*; Laboratoire de Chimie Théorique, Université de Paris VI: Paris, France, 1998.
(62) Silvi, B.; Savin, A. *Nature* **1994**, *371*, 683.
(63) Savin, A.; Silvi, B.; Colonna, F. *Can. J. Chem.* **1996**, *74*, 1088.
(64) Chesnut, D. B. *Chem. Phys.* **2001**, *271*, 9.

Table 7. NBO Atomic Charges, Mayer Atomic Orbital Valencies, Atomic Orbital Overlap-Weighted Bond Orders between Atoms, NRT Valencies (Covalencies), and Summaries of NRT Lewis Structures in XeO_2F_2 (C_{2v}), XeO_2F^+ (C_s), IO_2F (C_s), TeO_2F^- (C_s), and $FO_2XeFXeO_2F^+$ (C_1)[a]

XeO_2F_2 (C_{2v})

atom	charge	valency	natural valency (covalency)	bond	bond order
Xe	3.003	2.369	3.638 (1.687)	Xe−O(1); Xe−O(2)	0.871
O(1); O(2)	−0.897	0.809	1.037 (0.653)	Xe−F(1); Xe−F(2)	0.313
F(1); F(2)	−0.604	0.282	0.782 (0.190)		

natural Lewis[b] NBO	3.0% non-Lewis NBO population	total contribution	% s	% p	% d	% f
σ[Xe−O(1),O(2)]	1.96	12% Xe	10.5	76.0	11.7	1.78
		88% O	0.09	99.3	0.57	
σ[Xe−F(1),F(2)]	1.86	14% Xe	14.4	57.2	27.7.0	0.68
		86% F	5.71	94.1	0.17	
LP [Xe]	1.97	100% Xe	72.5	27.2	0.26	0.03

XeO_2F^+ (C_s)

atom	charge	valency	natural valency (covalency)	bond	bond order
Xe	2.890	2.148	2.648 (1.630)	Xe−O(1); Xe−O(2)	0.893
O(1); O(2)	−0.700	0.848	1.485 (0.872)	Xe−F	0.362
F	−0.490	0.322	0.310 (0.112)		

natural Lewis[b] NBO	2.8% non-Lewis NBO population	total contribution	% s	% p	% d	% f
σ[Xe−O(1)]	1.83	14% Xe	7.22	47.1	37.9	7.73
		86% O	0.54	98.8	0.70	
π[Xe−O(1)]	1.89	9% Xe	4.93	47.9	37.2	9.91
		91% O	0.31	99.0	0.68	
σ[Xe−O(2)]	1.95	14% Xe	6.84	80.4	10.1	2.64
		86% O	0.30	99.0	0.68	
π[Xe−O(2)]	1.75	29% Xe	16.6	55.2	22.0	6.11
		71% O	8.11	90.9	0.97	
σ[Xe−F]	1.76	14% Xe	9.15	50.4	30.8	9.58
		86% F	3.68	96.1	0.24	
LP[Xe]	1.98	100% Xe	74.3	25.5	0.10	0.02

IO_2F (C_s)

atom	charge	valency	natural valency (covalency)	bond	bond order
I	2.525	1.992	3.845 (1.345)	I−O(1); I−O(2)	0.838
O(1); O(2)	−0.952	0.801	1.290 (0.624)	I−F	0.316
F	−0.622	0.279	1.264 (0.098)		

natural Lewis[b] NBO	2.6% non-Lewis NBO population	total contribution	% s	% p	% d
σ[I−O(1),O(2)]	1.88	8% I	7.51	49.5	43.0
		92% O	2.20	97.3	0.47
π[I−O(1),O(2)]	1.89	10% I	4.06	65.8	30.1
		90% O	0.16	99.4	0.46
σ[I−F]	1.79	9% I	26.8	43.0	30.2
		91% F	6.84	93.0	0.19
LP[I]	1.98	100% I	75.6	24.2	0.14

TeO_2F^- (C_s)

atom	charge	valency	natural valency (covalency)	bond	bond order
Te	2.131	1.862	3.234 (1.072)	Te−O(1); Te−O(2)	0.754
O(1); O(2)	−1.202	0.754	1.399 (0.481)	Te−F	0.264
F	−0.728	0.264	0.500 (0.110)		

natural Lewis[b] NBO	7.2% non-Lewis NBO population	total contribution	% s	% p	% d
σ[Te−O(1)]	1.94	7% Te	15.8	69.8	14.3
		93% O	6.65	93.0	0.32
π[Te−O(1)]	1.90	22% Te	33.6	63.6	2.77
		78% O	10.4	89.2	0.44
σ[Te−O(2)]	1.93	6% Te	25.7	54.5	19.8
		94% O	6.69	93.0	0.32
π[Te−O(2)]	1.93	10% Te	4.38	88.6	7.00
		90% O	0.99	98.7	0.33
LP[Te]	1.98	100% Te	74.6	25.1	0.30

Table 7. Cont'd.

$FO_2XeFXeO_2F^+$ (C_1)

atom	charge	valency	natural valency (covalency)	bond	bond order
Xe(1); Xe(2)	2.979	2.422	3.000 (2.092)	Xe(1)−O(1); Xe(2)−O(3)	0.936
O(1); O(3)	−0.799	0.881	1.000 (0.775)	Xe(1)−O(2); Xe(2)−O(4)	0.934
O(2); O(4)	−0.804	0.881	1.000 (0.776)	Xe(1)−F(1); Xe(2)−F(2)	0.397
F(1); F(2)	−0.519	0.362	1.000 (0.542)	Xe(1)−F(3); Xe(2)−F(3)	0.147
F(3)	−0.714	0.260	0.000 (0.000)		

$FO_2XeFXeO_2F^+$ (C_1)

natural Lewis[b] NBO	3.2% non-Lewis NBO population	total contribution	% s	% p	% d	% f
σ[Xe(1)−O(1),O(2)]	1.96	13% Xe	10.7	80.1	7.42	1.79
		87% O	0.20	99.1	0.64	
σ[Xe(2)−O(3),O(4)]	1.96	13% Xe	10.8	80.2	7.23	1.75
		87% O	0.19	99.2	0.64	
σ[Xe(1)−F(1)]	1.92	26% Xe	1.46	95.3	2.62	0.59
		74% F	4.88	94.9	0.23	
σ[Xe(2)−F(2)]	1.92	26% Xe	1.46	95.3	2.62	0.59
		74% O	4.88	94.9	0.23	
LP[Xe(1),Xe(2)]	1.97	100% Xe	74.7	25.2	0.12	0.02

[a] MP2/Stutt RLC ECP. [b] For details, see Table S8 in the Supporting Information.

Gillespie rationale.[65] The unsymmetrical electron density distribution is also reflected in the shape of the *C*(Xe) core basin depicted in Figure 5.

(ii) XeO_2F^+, IO_2F, and TeO_2F^-. The natural charge on the central atom decreases with the decreasing formal oxidation number of the central atom: 2.89, XeO_2F^+ > 2.52, IO_2F > 2.13, TeO_2F^-. Like XeO_2F_2, the natural charge on the central atom is approximately half that of the formal oxidation number in this series, indicating that the bonding is very similar in all four species. As expected, the negative charges on the electronegative F and O ligands increase as the net charge of the species goes from +1 to −1. The oxygen double bonding is supported by high natural oxygen-to-central atom bond orders, which decrease in the series XeO_2F^+ (0.893) > IO_2F (0.838) > TeO_2F^- (0.754).

For XeO_2F^+ (IO_2F), the Xe^I−O double-bonded and Xe^I−F single-bonded natural Lewis structures [2.8% (2.6%) non-Lewis-type electrons] describe the bonding only marginally better than the Xe^I−O double-bonded structures, with ionic Xe^I−F bonded structures [2.9% (2.7%) non-Lewis-type electrons] providing an almost equal weighting of both resonance structures. For TeO_2F^-, the order is reversed: the Te−O double-bonded structure with no covalent Te−F bond (1.8% non-Lewis-type electrons) is somewhat favored over the double-bonded Te−O/single-bonded Te−F structure (4.1% non-Lewis-type electrons). The E−O (E = Xe, I, Te) double-bonded structures are supported by rather high natural valencies at O [XeO_2F^+ (1.48) > IO_2F (1.29) < TeO_2F^- (1.40)], while natural valencies on F are low [XeO_2F^+, 0.11; IO_2F, 0.10; TeO_2F^-, 0.11], indicating highly ionic E−F bonds across the series.

The semi-ionic bonding descriptions of the aforementioned species are supported by ELF basin population analyses, which show no bisynaptic bonding basins among these isoelectronic series, with their valence electrons mostly populating the oxygen and fluorine monosynaptic nonbonding (lone-pair) basins so that the *V*(E) (E = Te, I, Xe) basin lobes are very similar to each other (Figure 5). The lone-pair basins *V*(E) of the central atoms have high electron populations that increase in the order TeO_2F^- (2.99) < IO_2F (3.03) < XeO_2F^+ (3.26), while the corresponding basin volumes follow the reverse trend, TeO_2F^- (166.8) > IO_2F (126.4) > XeO_2F^+ (103.4). The increasing nuclear charges and electronegativities on going from Te to Xe are consistent with the aforementioned trends.

(iii) $FO_2XeFXeO_2F^+$. There is essentially no difference between the natural charges and bond orders of $FO_2XeFXeO_2F^+$ rotamers having C_s or C_1 symmetries. The Xe natural charges (2.98) are somewhat higher than those in XeO_2F^+. The bridging F_b atom has a more negative charge (−0.71) than the terminal F ligand (−0.52). Correspondingly, the Xe−F_t bond orders (0.40) are normal for single bonds, and the Xe- - -F_b bond order (0.15) is substantially less. The Xe−O bond order (0.94) is similar to those of other species discussed here and consistent with a high degree of double-bond character.

In the NBO analysis, the bonding in $FO_2XeFXeO_2F^+$ can be described by either an ionic model, $[FO_2Xe^+][F^-][^+XeO_2F]$ (valence bond resonance structure II), which provides a natural Lewis structure (3.2% non-Lewis-type electrons), or by the fully covalent model, $[FO_2XeFXeO_2F]^+$, having very weak covalent Xe- - -F bridge bonds (bond order, 0.13). The covalent model is equally satisfactory (3.3% non-Lewis-type electrons) when compared with the ionic description. The intermediate bonding description $[FO_2XeF][XeO_2F^+]$ (valence bond structures I and III) is likewise equally satisfactory (3.2% non-Lewis-type electrons), although it is a transition state in the NBO analysis. Overall, the NBO analyses indicate that the bonding in $FO_2XeFXeO_2F^+$ is more on the ionic side, with only weak covalent character for the bridging Xe- - -F bonds. Surprisingly, the NRT analysis gives ionic structure II as the 100% favored resonance structure.

(65) Gillespie, R. J.; Robinson, E. A. *Angew. Chem., Int. Ed. Engl.* **1996**, *35*, 495.

The ionic model $[FO_2Xe^+][F^-][^+XeO_2F]$ is further supported by the ELF analysis. The data for other basins are very similar to those of XeO_2F^+, but the bridging F atom is associated with only one, highly populated (7.62), nonbonding basin $V(F_3)$ having a volume of 89.7, which is of the same order as the total volume of $V_1(Xe)$ and $V_2(Xe)$, 90.7. Again, the basin lobes around both Xe atoms resemble those of XeO_2F_2 and $XeO_2(OTeF_5)_2$ (Figure 5) and give rise to F−Xe- - -F angles that are bent toward the xenon electron lone pairs.

Conclusions

The structures of the XeO_2F^+ and the fluorine-bridged $FO_2XeFXeO_2F^+$ cations in their crystal structures are based upon trigonal-pyramidal and trigonal-bipyramidal arrangements, respectively, in accordance with the VSEPR rules. The primary coordination spheres about the xenon atoms of $FO_2XeFXeO_2F^+$ closely resemble those of XeO_2F_2. Inclusion of secondary contacts results in distorted monocapped octahedral coordination spheres about xenon in XeO_2F^+ and $FO_2XeFXeO_2F^+$, from which the free valence electron pair of xenon may be inferred to occupy the capping position. Bending of the F−Xe−F or O−Xe−O angles toward the xenon valence electron lone-pair domains in XeO_2F_2, $XeO_2(OTeF_5)_2$, and $FO_2XeFXeO_2F^+$ implies that the repulsive effects of two equatorial oxygen double-bond domains on their axial F−Xe−F (O−Xe−O) angles are greater than that of a single electron lone pair. The ELF analyses provide semiquantitative, but more visual, bonding descriptions, which are in agreement with the experimental observations. The bending of the axial F−Xe−F (O−Xe−O) angle toward the lone pair of xenon results from the large Xe−O double-bond basins and the shape of the xenon lone-pair basin, which is more diffuse in the O−Xe−O equatorial plane than along the F−Xe−F (O−Xe−O) axial plane. While the experimentally confirmed E−O (E = Xe, I, Te) double-bond characters of XeO_2L_2, XeO_2L^+, IO_2F, TeO_2F^-, and $FO_2XeFXeO_2F^+$ (L = F, $OTeF_5$) are not fully represented by any single localized Lewis structure, NBO bonding descriptions lead to resonance combinations comprised of several different single- and double-bonded E−O natural Lewis structures in which the double-bonded contributors dominate.

Although XeO_2F^+ and $FO_2XeFXeO_2F^+$ salts can be synthesized from XeO_2F_2 and MF_5 at low temperatures in HF solvent, thermochemical calculations establish that these reactions are not spontaneous under standard conditions. These salts, once formed, are kinetically stable toward dissociation to XeO_2F_2 and MF_5 with the exception of $[XeO_2F][AsF_6]$, which readily dissociates to $[FO_2XeFXeO_2F][AsF_6]$ and AsF_5 under dynamic vacuum at 0 °C. While having significant kinetic stabilities at room temperature, the decompositions of XeO_2F^+ salts to XeF^+ salts and O_2 are significantly exothermic and are dominated by the large gas-phase enthalpy of decomposition for XeO_2F^+ (eq 8).

Experimental Section

Apparatus and Materials. Volatile materials were handled using vacuum lines constructed of nickel, stainless steel, and hexafluoropropylene−tetrafluoroethylene copolymer (FEP), and nonvolatile materials were handled in the atmosphere of a drybox.[66] All preparative work was carried out in previously dried and fluorine-passivated $^1/_4$-in.-o.d. FEP reaction vessels equipped with 316 stainless steel Whitey ORM2 valves, whereas crystal growth was carried out in similar vessels, which had a second $^1/_4$-in.-o.d. length of FEP tubing fused perpendicular to it ca. $^1/_3$ of the distance from the valve to give a T-shaped reaction vessel. Samples were stored in valved FEP vessels at −78 °C under dry Ar or N_2 until use.

Arsenic pentafluoride was prepared as previously described[7] and was used without further purification. Xenon hexafluoride was prepared from xenon (99.995%, Air Products and Chemicals, Inc.) and fluorine (Air Products and Chemicals, Inc.) using a modification[7] of the method described by Malm and Chernick[67] and purified by the reaction of small amounts of XeF_4 contaminant by fusion of the sample with KrF_2 in an FEP vessel at ca. 45 °C. Anhydrous HF (Harshaw Chemicals Co.) was purified by the standard literature method.[68] Antimony trifluoride (99.8%, Aldrich Chemical Co.) was sublimed under dynamic vacuum at ca. 200 °C prior to use and stored in a dry PFA bottle inside a drybox until use. Fluorine gas (Air Products and Chemicals Inc.) and H_2O (HPLC grade, Caledon) were used without further purification. Antimony pentafluoride was synthesized in situ by direct fluorination of SbF_3 with F_2 in anhydrous HF as previously described.[66] The compound $[H_3O][SbF_6]$ was prepared in HF solution by the reaction of SbF_5 with H_2O as previously described.[69]

α- and β-[XeO_2F][SbF_6]. Inside a drybox, SbF_3 (0.1936 g, 1.083 mmol) was loaded into an FEP reactor and ca. 0.5 mL of HF was condensed into the tube at −196 °C. Antimony trifluoride was directly fluorinated at room temperature using F_2 gas. The sample was then transferred to a drybox, where 35 μL of H_2O was syringed into the precooled tube at ca. −140 °C. The sample was warmed to room temperature and transferred to a metal vacuum line, where XeF_6 (0.2410 g, 0.9824 mmol) was condensed onto the $HF/SbF_5/H_2O$ mixture at −196 °C, followed by warming to −78 °C, where it was thoroughly mixed, giving a colorless solution. The solvent was removed by pumping on the solution for ca. 30 min at −78 °C, followed by further pumping for 30 min at 0 °C, yielding a white microcrystalline powder.

For the preparation of β-$[XeO_2F][SbF_6]$, XeF_6 (0.2579 g, 1.051 mmol) was initially condensed, at −196 °C, into a previously weighed FEP reaction vessel attached to a Kel-F valve. In the drybox, H_2O (0.0379 g, 2.101 mmol) was transferred into a T-shaped FEP reaction vessel followed by successive condensations on a metal vacuum line of ca. 0.3 mL of anhydrous HF onto the sample at −78 °C and XeF_6 at −196 °C. The reactor and contents were allowed to briefly warm to room temperature to effect dissolution and reaction and were then cooled to and stored at −78 °C until use. In the drybox, SbF_3 (0.5635 g, 3.153 mmol) was transferred to a second FEP reaction vessel. Approximately 0.3 mL of HF was condensed onto the sample, and SbF_5 was generated by direct fluorination of SbF_3 with F_2. Both reaction vessels were transferred to a drybox through a cold well maintained at ca. −140 °C, cut open, and connected through a Teflon Swagelok union. The SbF_5/HF solution was allowed to warm to room temperature and was quickly poured through the Teflon union connection into the XeO_2F_2/HF reaction vessel that was maintained at ca. −140 °C inside a cold well. The reaction mixture was allowed to warm to

(66) Casteel, W. J.; Dixon, D. A.; Mercier, H. P. A.; Schrobilgen, G. J. *Inorg. Chem.* **1996**, *35*, 4310.
(67) Malm, J. G.; Chernick, C. L. *Inorg. Synth.* **1966**, *8*, 258.
(68) Emara, A. A. A.; Schrobilgen, G. J. *Inorg. Chem.* **1992**, *31*, 1323.
(69) Christe, K. O.; Schack, C. J.; Wilson, R. D. *Inorg. Chem.* **1975**, *14*, 2224.

room temperature to effect dissolution, and upon cooling to −78 °C, a pale-yellow solid precipitated from solution. The Raman spectrum of the precipitate was recorded under a HF solvent at −78 °C, and the sample was subsequently stored at −78 °C until it could be redissolved and crystallized. When the synthesis was carried out in the same manner using 1:2, 1:3, and 1:4 molar ratios of XeO_2F_2/SbF_5, only β-$[XeO_2F][SbF_6]$ crystallized, as confirmed from crystallographic unit cell determinations.

$[XeO_2F][AsF_6]$ and $[FO_2XeFXeO_2F][AsF_6]$. Inside a drybox, 0.0223 g (1.24 mmol) of H_2O was syringed into a $^1/_4$-in.-o.d. T-shaped FEP reaction vessel, which had a Kel-F valve fitted to the side arm. Anhydrous HF (ca. 0.5 mL) was then distilled onto the H_2O at −78 °C, followed by condensation of XeF_6 (0.1521 g, 0.6200 mmol) onto the H_2O/HF sample at −196 °C such that it condensed above the frozen HF solvent. The sample was then warmed, with mixing, to ca. 0 °C to effect dissolution of XeF_6. Arsenic pentafluoride (0.1264 g, 0.744 mmol) was condensed into the reaction mixture at −196 °C, warmed to ca. 0 °C, and thoroughly mixed. Upon cooling of the sample to −78 °C, a very pale-yellow precipitate formed and was confirmed to be $[XeO_2F][AsF_6]$ by recording the Raman spectrum[9] at −78 °C under HF solvent. The sample was stored at −78 °C until it could be redissolved and crystallized.

In the drybox, 0.0254 g (1.41 mmol) of H_2O was transferred into a FEP reaction vessel and 0.5 mL of HF was condensed onto the H_2O at −78 °C. Xenon hexafluoride (0.1731 g, 0.7058 mmol) was condensed into the sample tube at −196 °C such that it was deposited above the frozen H_2O/HF solution. The sample was then slowly warmed to ca. 0 °C to effect the dissolution of XeF_6 by slowly leaching it off of the reactor walls. Once XeF_6 had dissolved, AsF_5 (9.29 mmol) was condensed into the reaction vessel at −196 °C and was warmed to 0 °C to effect dissolution. The sample was then cooled to −78 °C, pumped for 35 min to remove excess AsF_5 and HF solvent, and pumped for a further 35 min at 0 °C to give a white, crystalline solid. The Raman spectrum revealed that the dry sample was mainly $[FO_2XeFXeO_2F][AsF_6]$ (77%) and $[XeO_2F][AsF_6]$ (23%). The sample was pumped for an additional 1 h at 0 °C, after which the Raman spectrum showed that it was pure $[FO_2XeFXeO_2F][AsF_6]$.[9]

$[XeF_5][SbF_6]\cdot XeOF_4$. In the drybox, 0.5454 g (2.141 mmol) of $[H_3O][SbF_6]$ was loaded into a $^1/_4$-in. FEP reaction vessel. Anhydrous HF was condensed into the reaction vessel (ca. 0.3 mL) at −78 °C. A preweighed amount of XeF_6 (0.2625 g, 1.070 mmol) was then condensed into the reaction vessel at −196 °C, and the reactants were dissolved by warming the reaction vessel to −78 °C. A white, microcrystalline product was obtained upon pumping off solvent at −78 to −50 °C, which was stable at room temperature. The sample was stored under dry N_2 at −78 °C until it could be characterized by Raman spectroscopy and by ^{19}F and ^{129}Xe NMR spectroscopy in HF solvent.

Crystal Growth. Approximately 100−150 mg of solid α-$[XeO_2F][SbF_6]$, $[FO_2XeFXeO_2F][AsF_6]$, or $[XeF_5][SbF_6]\cdot XeOF_4$ was loaded into a T-shaped $^1/_4$-in.-o.d. FEP reaction vessel inside a drybox, and approximately 0.5 mL of HF was condensed onto the solid at −78 °C. The solids were dissolved at ca. 0 °C, and the samples were immediately cooled to −20 to −25 °C. In the case of $[XeO_2F][AsF_6]$, a 1:1 mixture of XeO_2F_2 and AsF_5 in HF that had been prepared earlier (vide supra) was warmed to 0 °C to effect dissolution of precipitated $[XeO_2F][AsF_6]$ and then immediately cooled to −40 °C just prior to crystal growth. In the case of β-$[XeO_2F][SbF_6]$, a 1:2 stoichiometric mixture of XeO_2F_2 and SbF_5 in HF solvent (vide supra) was concentrated at −78 °C by removal of HF solvent under dynamic vacuum, resulting in the formation of a pale-yellow precipitate. The sample was then allowed to warm until the precipitate had dissolved (ca. 0 °C) and was then cooled to −20 °C. Slow crystal growth was induced by further cooling of the samples, at varying rates, to between −45 and −50 °C over several hours, after which time no further crystal growth was apparent (in the case of $[FO_2XeFXeO_2F][AsF_6]$, the crystallization was continued until −70 °C). The temperature was then lowered to −78 °C over a period of 1 h without additional crystallization. Crystalline material was isolated by decantation of the HF solvent into the side arm of the reaction vessel, which had been cooled to −196 °C. Residual HF was removed under dynamic vacuum at −78 °C. The side arm of the reaction vessel, with its contents at −196 °C, was heat-sealed under dynamic vacuum and removed. The crystalline samples were stored at −78 °C until a suitable crystal could be mounted on the X-ray diffractometer.

Raman Spectroscopy. The low-temperature Raman spectra were recorded on a Bruker RFS 100 FT-Raman spectrometer using 1064-nm excitation as previously described.[70]

X-ray Structure Determinations of α- and β-$[XeO_2F][SbF_6]$, $[XeO_2F][AsF_6]$, $[FO_2XeFXeO_2F][AsF_6]$, and $[XeF_5][SbF_6]\cdot XeOF_4$. Collection and Reduction of X-ray Data. Crystals were mounted under a flow of cold nitrogen at ca. −115 °C as previously described.[70] The diffraction data for α-$[XeO_2F][SbF_6]$, β-$[XeO_2F][SbF_6]$, $[XeO_2F][AsF_6]$, $[FO_2XeFXeO_2F][AsF_6]$, and $[XeF_5][SbF_6]\cdot XeOF_4$ were collected using a P4 Siemens diffractometer, equipped with a SMART 1K charge-coupled device (CCD) area detector (using the program *SMART*)[71] and a rotating anode using graphite-monochromated Mo Kα radiation (λ = 0.710 73 Å). The crystal-to-detector distance was 5.0140 cm for α-$[XeO_2F][SbF_6]$ and $[FO_2XeFXeO_2F][AsF_6]$, 5.0120 cm for $[XeO_2F][AsF_6]$, 4.9870 cm for β-$[XeO_2F][SbF_6]$, and 4.9920 cm for $[XeF_5][SbF_6]\cdot XeOF_4$. The data collections were carried out in a 512 × 512 pixel mode using 2 × 2 pixel binning. Complete spheres of data were acquired for α-$[XeO_2F][SbF_6]$, β-$[XeO_2F][SbF_6]$, $[FO_2XeFXeO_2F][AsF_6]$, and $[XeF_5][SbF_6]\cdot XeOF_4$ to better than 0.8 Å resolution, consisting of a typical full ψ rotation at $\chi = 0°$ using (1200 + 50) 0.3° frames, followed by a series of short (100 frames) ω scans at various χ and ψ settings to fill the gaps, with the exception of $[XeO_2F][AsF_6]$. The data for $[XeO_2F][AsF_6]$ were acquired using a full ψ rotation at $\chi = 0°$ using (1000 + 40) 0.36° frames, followed by a series of short (80 frames) ω scans at various χ and ψ settings to fill the gaps. A complete data set was acquired at a 2θ setting of 332°, and an additional sphere of high angle data (2θ at 315°) was also acquired. For α-$[XeO_2F][SbF_6]$ and $[XeF_5][SbF_6]\cdot XeOF_4$, an additional sphere of data was acquired at high angle with 2θ at 345°. The raw diffraction data sets were integrated and scaled using *SAINT+*[72] and *SADABS*.[73]

Solution and Refinement of the Structures. The unit cell dimensions and space groups for all structures were determined using the program XPREP.[74] All solutions were obtained using direct methods that located the Xe, As, and Sb atoms. Successive difference Fourier syntheses revealed the positions of the fluorine and oxygen atoms. The final refinements were obtained by introduction of anisotropic thermal parameters for all of the atoms

(70) Gerken, M.; Dixon, D. A.; Schrobilgen, G. J. *Inorg. Chem.* **2000**, *39*, 4244.
(71) *SMART*, version 5.611; Siemens Energy and Automotive Analytical Instrumentation: Madison, WI, 1999.
(72) *SAINT+*, version 6.02; Siemens Energy and Automotive Analytical Instrumentation: Madison, WI, 1999.
(73) Sheldrick, G. M. *SADABS* (Siemens Area Detector Absorption Corrections), version 2.03; Bruker AXS, Inc.: Madison, WI, 1999.
(74) Sheldrick, G. M. *SHELXTL-Plus*, version 5.1; Siemens Analytical X-ray Instruments Inc.: Madison, WI, 1998.

and by introduction of a secondary extinction parameter and a weighting factor recommended by the refinement program.

The β-$[XeO_2F][SbF_6]$ structure was refined in a manner analogous to that of the α-phase. However, as a result of the crystallographically imposed symmetry at the fluorine and oxygen positions, which resulted in a population disorder of these sites, the model was adjusted to refine fluorine at a 33.3% statistical probability, with the balance being applied to oxygen for these sites.

Although the structure of $[XeO_2F][AsF_6]$ was solved in the orthorhombic system in the chiral space group $P2_12_12_1$, it crystallized as a racemic twin. The solution of the structure was further complicated by the presence of cubic twinning. This multiple twinning, and the consequent fluorine and oxygen population disorder, precluded accurate geometric parameters from being obtained. In the solution of $[XeO_2F][AsF_6]$, the twin law (0 1 0 0 0 1 1 0 0 −6) was applied to account for cubic twinning as well as chiral twinning.

Electronic Structure Calculations. Geometries were fully optimized at the HF, SVWN, and MP2 levels of theory using a DZVP basis set[75] and a Stuttgart RLC ECP basis set[75] with two polarization functions.[76] Fundamental vibrations were calculated and NBO analyses[54−57] were performed for the optimized local minima. All MO calculations were done using the *Gaussian 98* program package.[77] ELF calculations were performed at the HF/DZVP level using the *TopMod program package*.[54] The *TopMod package* sacrifices some accuracy for efficiency and, according to the authors,[78] is thought to be accurate to a few percent, sufficient for comparative studies. This accuracy implies the use of integration grids with a step size not larger than 0.1 au.

Acknowledgment. This paper is dedicated to our friend and colleague Professor Karl O. Christe on the occasion of his 70th birthday. We thank the Natural Sciences and Engineering Research Council of Canada for support in the form of a research grant. We also thank McMaster University for the award of a James A. Morrison Memorial Scholarship and the Ontario Ministry of Education and Training for the award of an Ontario Graduate Scholarship (B.E.P.). We thank Dr. Hélène P. A. Mercier for her assistance in preparing and critiquing this manuscript.

Supporting Information Available: Thermochemistry, HF solvation of XeO_2F^+; computational results; NRT, NBO, and ELF analyses (complementary discussion); thermochemical cycles describing the reactions of XeO_2F_2 with MF_5 (M = As, Sb) (Figure S1); calculated geometries of the $XeO_2F^+ \cdot xHF$ adducts (Figure S2); bond lengths and bond angles for XeO_2F^+, IO_2F, ClO_2F, and TeO_2F^- (Table S1); electronic energies and Gibbs free energies for the calculated species (Table S2); standard entropies for equations A−I in Table 3 (Table S3); experimental and calculated vibrational data for XeO_2F_2 (Table S4), α-XeO_2F^+, IO_2F, and TeO_2F^- (Table S5), and $FO_2XeFXeO_2F^+$ (Table S6); experimental and calculated geometrical parameters (Table S7); three best natural Lewis structures derived from NBO analyses (Table S8), NBO parameters (Table S9), and ELF parameters (Table S10) for XeO_2F_2 (C_{2v}), XeO_2F^+ (C_s), IO_2F (C_s), TeO_2F^- (C_s), $FO_2XeFXeO_2F^+$ (C_1) $XeO_2(OTeF_5)_2$ (C_1), and $XeO_2(OTeF_5)^+$ (C_1); X-ray crystallographic files (CIF format) for the structure determinations of α- and β-$[XeO_2F][SbF_6]$, $[XeO_2F][AsF_6]$, $[FO_2XeFXeO_2F][AsF_6]$, and $[XeF_5][SbF_6] \cdot XeOF_4$. This material is available free of charge via the Internet at http://pubs.acs.org.

IC0510260

(75) Basis sets were obtained from the Extensible Computational Chemistry Environment Basis Set Database, version 2/25/04, as developed and distributed by the Molecular Science Computing Facility, Environmental and Molecular Science Laboratory, which is part of the Pacific Northwest Laboratory, P.O. Box 999, Richland, WA 99352.

(76) Huzinaga, S.; Andzelm, J.; Klobukowski, M.; Radzio-Andzelm, E.; Sakai, Y.; Tatewaki, H. *Gaussian Basis Sets for Molecular Calculations*; Physical Science Data 16; Elsevier: Amsterdam, The Netherlands, 1984.

(77) Frisch, M. J.; Trucks, G. W.; Schlegel, H. B.; Scuseria, G. E.; Robb, M. A.; Cheeseman, J. R.; Zakrzewski, V. G.; Montgomery, J. A., Jr.; Stratmann, R. E.; Burant, J. C.; Dapprich, S.; Millam, J. M.; Daniels, A. D.; Kudin, K. N.; Strain, M. C.; Farkas, O.; Tomasi, J.; Barone, V.; Cossi, M.; Cammi, R.; Mennucci, B.; Pomelli, C.; Adamo, C.; Clifford, S.; Ochterski, J.; Petersson, G. A.; Ayala, P. Y.; Cui, Q.; Morokuma, K.; Malick, D. K.; Rabuck, A. D.; Raghavachari, K.; Foresman, J. B.; Cioslowski, J.; Ortiz, J. V.; Stefanov, B. B.; Liu, G.; Liashenko, A.; Piskorz, P.; Komaromi, I.; Gomperts, R.; Martin, R. L.; Fox, D. J.; Keith, T.; Al-Laham, M. A.; Peng, C. Y.; Nanayakkara, A.; Gonzalez, C.; Challacombe, M.; Gill, P. M. W.; Johnson, B. G.; Chen, W.; Wong, M. W.; Andres, J. L.; Head-Gordon, M.; Replogle, E. S.; Pople, J. A. *Gaussian 98*, revision A.11; Gaussian, Inc.: Pittsburgh, PA, 1998.

(78) Noury, S.; Krokidis, X.; Fuster, F.; Silvi, B. *Comput. Chem.* **1999**, *23*, 597.